UNIVERSITY OF TWENTE.

Amsterdam UMC
University Medical Centers

Subhairline Electroencephalography for the Detection of Large Vessel Occlusion Stroke

A thesis submitted for the Master's degree in Technical Medicine

by

Eva Anna Groenendijk

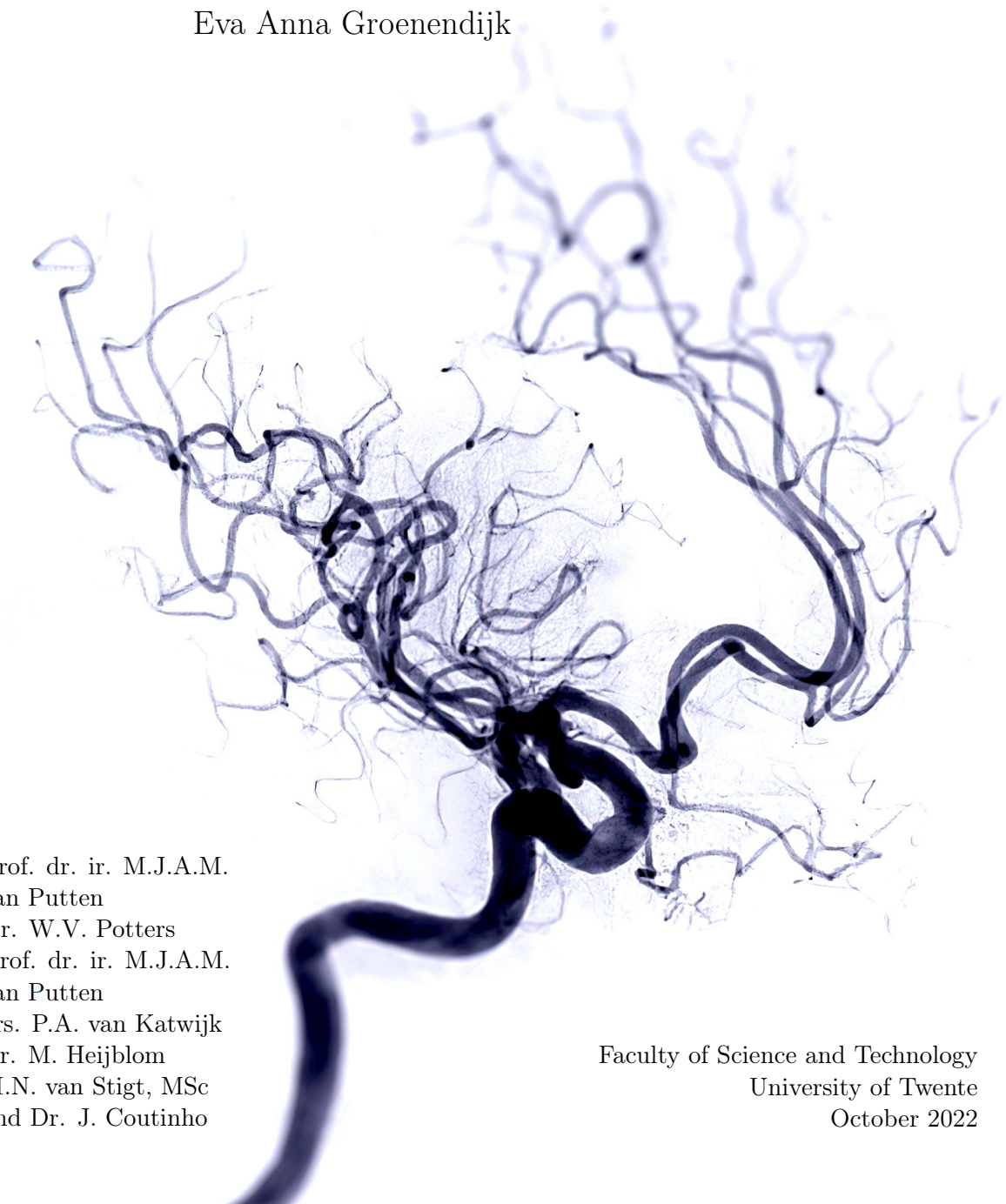

Graduation committee

Chairman:	Prof. dr. ir. M.J.A.M. van Putten
Medical supervisor:	Dr. W.V. Potters
Technical supervisor:	Prof. dr. ir. M.J.A.M. van Putten
Process supervisor:	drs. P.A. van Katwijk
External member:	Dr. M. Heijblom
Additional members:	M.N. van Stigt, MSc and Dr. J. Coutinho

Faculty of Science and Technology
University of Twente
October 2022

Abstract

Introduction: Endovascular thrombectomy (EVT) for large vessel occlusion stroke of the anterior circulation (LVO-a) can only be performed in selected hospitals. Of all EVT-eligible patients 45–83% are initially presented in a hospital incapable of EVT and need to be transferred. A resulting delay of 39–114 minutes in EVT initiation is associated with worse functional outcome. A prehospital triage instrument with which paramedics can reliably identify patients with an LVO-a stroke would enable direct routing of these patients to the right hospital. Research has shown that electroencephalography (EEG) can discriminate between patients with and without an LVO-a stroke. In this study, the diagnostic accuracy of subhairline EEG for LVO-a stroke was evaluated.

Methods: An EEG recording was performed in 37 patients who were presented to the emergency department with a suspected stroke or known LVO-a stroke, as soon as possible after presentation, and prior to potential EVT. Recordings were performed using 9 self-adhesive electrodes placed on the forehead and behind the ears. We evaluated the diagnostic accuracy of EEG features quantifying frequency band power (relative delta, theta, alpha and lower beta powers and power ratios), brain symmetry (pairwise derived Brain Symmetry Index [pdBSI]), connectivity (Magnitude Squared Coherence [MSC] and weighted phase lag index), complexity (sample entropy and Higuchi Fractal Dimension) and the probability distribution (skewness and kurtosis) for LVO-a stroke using receiver operating characteristic analysis. Optimal cut-off points were determined as the maximum sensitivity at a specificity of $\geq$ 80% for LVO-a stroke.

Results: Median age was 75 (IQR 66–81) years and 17/37 (46%) patients were female. In total, 13/37 (35%) patients had an LVO-a stroke, 14/37 (38%) a non-LVO-a ischemic stroke, 4/37 (11%) a transient ischemic attack and 6/37 (16%) a stroke mimic. Median onset-to-EEG-time was 250 (IQR 127–528) minutes and median EEG-recording-time was 185 (IQR 181-–189) seconds. Recordings of all patients were of sufficient quality to calculate frequency band power and brain symmetry measures. Connectivity measures could not be calculated for 1/13 (8%) LVO-a stroke patient. Highest diagnostic accuracy for LVO-a stroke detection was obtained by the pdBSI in the theta frequency band (AUC=0.88; sensitivity=85%; specificity=83%).

Conclusion: Subhairline EEG is a promising method for detection of LVO-a stroke, but validation in a larger study population and the prehospital setting is necessary.

Keywords: acute stroke, electroencephalography, prehospital triage

Table of Contents

List of Abbreviations

A1 first segment of the anterior cerebral artery.

AIS acute ischemic stroke.

ApEn approximate entropy.

API application programming interface.

AUC area under the receiver operating characteristic curve.

CBF cerebral blood flow.

DAR delta/alpha ratio.

DTABR (delta+theta)/(alpha+beta) ratio.

DTR delta/theta ratio.

ED emergency department.

EEG electroencephalography.

EVT endovascular thrombectomy.

HFD Higuchi's fractal dimension.

ICA independent component analysis.

IQR interquartile range.

IVT intravenous thrombolysis.

LOOCV Leave-One-Out Cross-Validation.

LR logistic regression.

LVO large vessel occlusion.

LVO-a large vessel occlusion of the anterior circulation.

M1 first segment of the middle cerebral artery.

M2 second segment of the middle cerebral artery.

MSC Magnitude Squared Coherence.

NIHSS National Institutes of Health Stroke Scale.

NPV negative predictive value.

pdBSI pairwise derived Brain Symmetry Index.

PLI phase lag index.

PPV positive predictive value.

ROC receiver operating characteristic.

rsBSI revised Brain Symmetry Index.

SampEn sample entropy.

SMOTE Synthetic Minority Oversampling Technique.

TAR theta/alpha ratio.

TIA transient ischemic attack.

UMC University Medical Centers.

wICA wavelet enhanced independent component analysis.

WPLI weighted phase lag index.

1 Introduction

Stroke is the second leading cause of death and third leading cause of disability worldwide [1–4]. The majority of all strokes are ischemic in nature [3, 5]. Of all patients presented with acute ischemic stroke (AIS), around 20% have a large vessel occlusion (LVO) [6, 7]. Endovascular thrombectomy (EVT) has become standard treatment for patients with an LVO of the anterior circulation (LVO-a), ever since its efficacy was established in five randomized trials in 2015 [8]. EVT, however, can only be performed in comprehensive stroke centers (CSCs) [8]. Of all EVT-eligible patients 45–83% are initially presented in a primary stroke center and need to be transferred to a CSC for EVT [9–12]. This interhospital transfer causes delays of 39–114 minutes in EVT initiation, which is associated with worse functional outcome [9, 10, 13–15].

Since EVT needs to be initiated as soon as possible, early identification of EVT-eligible patients in the prehospital setting and subsequent direct transport to the closest CSC will benefit the outcome of patients. Electroencephalography (EEG) is a promising technique for prehospital LVO-a stroke detection, as reduced cerebral blood flow (CBF) results in a decrease in higher frequencies, followed by an increase in lower frequencies [16–19]. Several studies have shown that EEG can discriminate between AIS patients and controls, and between LVO-a stroke patients and suspected stroke patients without an LVO-a stroke [19–25].

The use of conventional wet electrode EEG would not be feasible in the prehospital setting, as it can be time consuming [26]. An easy-to-use alternative with minimal setup time is needed. Possible alternatives that meet these requirements are a reduced EEG montage, a dry electrode EEG system [20, 21] or subhairline EEG [27]. In this research we focus on subhairline EEG, because it can be used in practically all patients, regardless of hairstyle and head size.

Subhairline EEG has never been investigated for the specific purpose of LVO-a stroke detection, but frontal and forehead EEG have been studied in patients with AIS. Finnigan et al. (2020) [27] for instance showed that F3–F4 delta/alpha ratio (DAR) values discriminated between 18 AIS patients and 28 healthy controls with high diagnostic accuracy (area under the receiver operating characteristic (ROC) curve=0.99; sensitivity=94%; specificity=93%). Hussain et al. (2020) [28] developed a portable device with dry electrodes at positions Fp1 and Fp2 and demonstrated a difference in revised Brain Symmetry Index (rsBSI), DAR, and delta/theta ratio (DTR) values between 37 ischemic stroke patients and 36 healthy controls. In two other studies by Gottlibe et al. (2020) [29] and Wilkinson et al. (2020) [30] an EEG headband (Muse, Interaxon Inc., Toronto, Canada) was used to explore forehead EEG in patients with AIS. Gottlibe et al. showed a difference between rsBSI values of 33 AIS patients and 25 healthy controls. Wilkinson et al. found differences in DAR, (delta+theta)/(alpha+beta) ratio (DTABR) and pairwise derived Brain Symmetry Index (pdBSI) values when comparing 16 patients with AIS and 9 controls. These EEG changes scale with the severity of the stroke.

The studies described above suggest that subhairline EEG could be used for LVO-a stroke detection. To gain more insight into subhairline EEG as triage instrument, we will answer the following research question in this thesis: *"What is the diagnostic accuracy of subhairline EEG for large vessel occlusion stroke of the anterior circulation in patients admitted to the emergency department with suspected stroke?"*. We hypothesize that subhairline EEG can be used to discriminate between LVO-a stroke patients and suspected stroke patients without an LVO-a stroke.

2 Background: The effect of LVO-a stroke on EEG signals

The functioning of the brain is closely tied to its blood supply [17, 31]. In normal conditions the CBF lies in the range of 50–70 mL blood per 100 g of brain tissue per minute [32, 33]. When the CBF drops below normal conditions, protein synthesis is inhibited [34]. At this stage no changes are seen in EEG signals; the first EEG abnormalities become present at a CBF of approximately 25–35 mL/100g/min [17]. Initially there is a decrease in the fast frequencies (in the alpha and beta frequency band) followed by an increase in the slow frequencies (in the delta and theta frequency band) when the CBF declines further [17, 33]. These EEG changes coincide with various cellular events, ranging from anaerobic glycolysis to the suppression of synaptic transmission [16, 17, 32, 34, 35]. Under the infarction threshold of 10–12 mL/100g/min the EEG becomes iso-electric [16, 17, 33, 36]. The affected neurons lose their membrane potential, start to swell, and become irreversibly damaged [16, 17, 34]. An overview of changes in EEG signals and cellular responses at different CBF values is given in Table 1.

Table 1: Changes in EEG signals and cellular responses at different CBF values. The CBF is expressed in mL blood per 100 g of brain tissue per minute.

CBF (mL/100g/min)	**EEG changes**	**Cellular response**	**Neuronal injury**
35-50	• No change	• Inhibition of protein synthesis	No injury
12-35	• Decrease of fast frequencies (alpha and beta) • Increase of slow frequencies (delta and theta)	• Anaerobic glycolysis • Complete suppression of protein synthesis • Suppression of synaptic transmission	Reversible[1]
<10-12	• Iso-electric EEG	• Anoxic depolarization • Cytotoxic edema	Not reversible[2]

[1] can be irreversible depending on the extent and duration of ischemia [37, 38].
[2] brainstem neurons depolarize more slowly and can recover [39].

2.1 Quantifying the effect of LVO-a stroke

Ischemia-induced changed in EEG signals can be quantified and used to distinguish patients with and without an LVO-a stroke. Studies in which EEG features values have been compared between either LVO-a stroke patients and other suspected stroke patients without LVO-a stroke or stroke patients and controls have been summarized in Tables 2 and 3.

2.1.1 Frequency band power based features

Features that are most often used to distinguish stroke patients from non-stroke patients are based on frequency band power. Ischemia causes slowing of the EEG and features that can be used to express this shift in frequencies are therefore very common for ischemic stroke detection.

2.1.1.1 Relative band powers

The simplest method of analyzing a shift in frequencies is quantifying the power of each EEG frequency band. The relative power of a specific band is subsequently calculated by dividing the spectral density in that band by the total spectral density or the spectral density in a wider range.

Table 2: A summary of the key details of past studies in which EEG features in (LVO-a) stroke patients have been analyzed.

Study	**Onset-to-EEG-time**	**Study population**	**EEG setup**	**Hemisphere**[1]	**EEG feature(s)**	**Results**[2]
Van Meenen & Van Stigt et al. [20]	Median = 4.4h	LVO-a stroke (n=9) vs AIS, TIA and stroke mimics (n=56)	8 channel dry electrode (FC3, FC4, CP3, CP4, FT7, FT8, TP7, and TP8)	Ipsilesional	Relative delta power Relative theta power Relative alpha power DAR TAR pdBSI WPLI	Median = 0.85 vs 0.80 (p=0.24); AUC=0.63 Median = 0.63 vs 0.49 (p=0.01); AUC=0.77 Median = 0.19 vs 0.28 (p<0.01); AUC=0.80 Median = 0.90 vs 0.84 (p=0.02); AUC=0.76 Median = 0.45 vs 0.26 (p<0.01); AUC=0.83 Median = 0.31 vs 0.33 (p=0.33); AUC=0.61 Median = 0.08 vs 0.10 (p=0.27); AUC=0.38
Erani et al. [21]	Median = 9.5h	LVO-a stroke[3] (n=7) vs Stroke, TIA and stroke mimics (n=93)	20 channel dry electrode	Ipsilesional and contralesional	Alpha, low and high beta power	Logistic regression model trained using EEG features: AUC=68.9%, Sensitivity=41%, Specificity=80%
Sergot et al. [22]	< 24h	LVO-a stroke (n=25) vs vs Stroke, TIA and stroke mimics (n=84)	13 channel wet electrode	Whole brain	Somatosensory evoked potentials and unknown EEG features	Automated binary classifier using EEG features and SSEP signals: Sensitivity=80%, Specificity=80%
Shreve et al. [23]	Median = 6.6h	Large AIS[4] (n=5) vs Stroke, TIA and stroke mimics (n=19)	256 channel wet electrode	Ipsilesional, contralesional and whole brain	Delta power Beta power ADR DTABR	OR = 0.91, 0.87, 0.88; p = 0.38, 0.04, 0.08 OR = 1.2, 1.27, 1.3; p = 0.18, 0.04, 0.07 OR = 686, 138135, 22695; p = 0.005, 0.0006, 0.01 OR = 0.0004, 1.0e-5, 1.8e-5; p = 0.11, 0.015, 0.03
Finnigan et al. [19]	< 24h	AIS[5] (n=18) vs Controls (n=28)	19 channel wet electrode	Whole brain	Relative delta power Relative theta power Relative alpha power Relative beta bower DAR DTABR $Q_{slowing}$[6]	Mean = 0.58 vs 0.29 (p<0.0001); AUC=0.99 Mean = 0.17 vs 0.11 (p<0.0001); AUC=0.81 Mean = 0.13 vs 0.34 (p<0.0001); AUC=0.97 Mean = 0.12 vs 0.26 (p<0.0001); AUC=0.90 Mean = 6.64 vs 1.34 (p<0.0001); AUC=1.00 Mean = 4.25 vs 0.84 (p<0.0001); AUC=1.00 Mean = 0.66 vs 0.36 (p<0.0001); AUC=0.97
Finnigan et al. [27]	< 24h	AIS[5] (n=18) vs Controls (n=28)	6 frontal wet electrodes	Whole brain	DAR for F3–F4	Sensitivity = 100%, specificity = 89%

ADR = alpha/delta ratio; AIS = acute ischemic stroke; AUC = area under the receiver operating characteristic curve; DAR = delta/alpha ratio; DTABR = (delta+theta)/(alpha+beta) ratio; h = hours; LVO-a = anterior circulation large vessel occlusion; OR = odds ratio; pdBSI = pairwise derived Brain Symmetry Index; SSEP = somatosensory evoked potentials; TAR = theta/alpha ratio; TIA = transient ischemic attack; WPLI = weighted phase lag index.

[1] the hemisphere for which the EEG features were calculated.

[2] the results are given respectively for the hemispheres for which the EEG features were calculated.

[3] all occlusions were located in the first segment of the middle cerebral artery.

[4] >20 mL of infarct volume.

[5] all patients had a stroke of the middle cerebral artery territory.

[6] $Q_{slowing}$ was defined as the ratio between the power across 1.95—7.81 Hz versus the power across 1.95-–24.90 Hz.

Table 3: A summary of the key details of past studies in which features in stroke patients have been analyzed.

Study	Onset-to-EEG-time	Study population	EEG setup	Hemisphere[1]	EEG feature(s)	Results[2]
Sheorajpanday et al. [24]	Median = 16h	Stroke (n=21) vs TIA and controls (n=20)	20 channel wet electrode	Whole brain	pdBSI	Higher in stroke patients (p=0.001)
Van Kaam et al. [25]	Median = 9h	Stroke[3] (n=18) vs controls (n=18)	20 channel wet electrode	Ipsilesional and contralesional	DAR	Higher for both hemispheres in stroke patients ($p \leq 0.001$)
					MSC[4]	Lower in the theta, alpha and beta bands for both hemispheres in stroke patients ($p \leq 0.05$)
					WPLI[4]	Lower in the alpha and beta bands for both hemispheres in stroke patients ($p \leq 0.05$)
Liu et al. [40]	< 7d	Ischemic thalamic stroke (n=12) vs controls (n=11)	22 channel wet electrode	Whole brain	SampEn	Higher in stroke patients ($p<0.05$ for 8 channels)
Rubega et al. [41]	Mean = 30h	Stroke (n=16) vs controls (n=11)	30 channel wet electrode (stroke patients), 256 channel wet electrode (controls)	Whole brain	HFD	Range = [1.0222, 1.0835] vs range = [1.1098, 1.3447] ($p<$1.62e-4)
Zappasodi et al. [42]	Mean = 5.4d	Stroke (n=36)[3] vs controls (n=19)	19 channel wet electrode	Whole brain	FD	Mean = 1.447 vs 1.525 ($p<0.007$)
Hussain et al. [28]	< 120h	Stroke (n=37) vs controls (n=36)	2 channel dry electrode (Fp1 and Fp2)	Ipsilesional and contralesional[5]	DAR	Mean = 5.556, 7.043 vs 3.634, 4.100 ($p<0.0005$)
					rsBSI	Mean = 0.263 vs 0.143 ($p<0.0001$)
					Skewness[4]	Lower in Fp1 for stroke patients ($p<0.05$)
					Kurtosis[4]	Lower in Fp2 for stroke patients ($p<0.05$)
Gottlibe et al. [29]	<48h	AIS (n=33) vs controls (n=25)	EEG headband[6]	Whole brain	rsBSI	Median = 0.363 vs 0.169 ($p<0.05$)
Wilkinson et al. [30]	Mean = 3.85d	AIS (n=16) vs stroke mimics (n=9)	EEG headband[6]	Ipsilesional and contralesional[5]	DAR DTABR pdSBI	Classification tree trained using EEG features: sensitivity = 63%, specificity = 86% and accuracy = 76%

d = days; DAR = delta/alpha ratio; FD = fractal dimension; h = hours; HFD = Higuchi's fractal dimension; MSC = Magnitude Squared Coherence; pdBSI = pairwise derived Brain Symmetry Index; rsBSI = revised Brain Symmetry Index; SampEn = sample entropy; TAR = theta/alpha ratio; TIA = transient ischemic attack; WPLI = weighted phase lag index.

[1] the hemisphere for which the EEG features were calculated.

[2] the results are given respectively for the hemispheres for which the EEG features were calculated.

[3] all patients had a stroke of the middle cerebral artery territory.

[4] feature was calculated in the delta, theta, alpha and beta frequency bands.

[5] the rsBSI or pdBSI was calculated for the whole brain.

[6] Muse, Interaxon Inc., Toronto, Canada.

2.1.1.2 Power ratios

Slowing of EEG signals caused by ischemia can also be quantified by the ratios between lower and higher frequency bands. Commonly used EEG features for this purpose are the DAR, theta/alpha ratio (TAR) and DTABR. These features are calculated using the following formulas:

$$\text{DAR} = \frac{P(\delta) - P(\alpha)}{P(\delta) + P(\alpha)}, \tag{1}$$

$$\text{TAR} = \frac{P(\theta) - P(\alpha)}{P(\theta) + P(\alpha)}, \tag{2}$$

$$\text{DTABR} = \frac{(P(\delta) + P(\theta)) - (P(\alpha) + P(\beta))}{(P(\delta) + P(\theta)) + (P(\alpha) + P(\beta))}, \tag{3}$$

where δ, θ, α and β represent the delta, theta, alpha and lower beta band respectively. The ratios are normalized between -1 and 1. A value between -1 and 0 indicates that the power of the higher frequencies (alpha and/or lower beta band) is greater than the lower frequencies (delta and/or theta band). For values between 0 and 1 the opposite is true.

2.1.2 Frequency asymmetry feature

An EEG feature that can be used to evaluate the difference in spectral characteristics between the left and right hemisphere is the pairwise derived Brain Symmetry Index (pdBSI) [24]. The severity of asymmetry in the EEG is determined by calculating the Fourier coefficients of the EEG signal along homologous channel pairs $i = 1, ..., M$ at frequency $j = 1, ..., N$ for the right and left hemisphere (R_{ij} and L_{ij} respectively). The pdBSI ranges between 0 (full symmetry) and 1 (maximal asymmetry) and is defined as:

$$\text{pdBSI} = \frac{1}{NM} \sum_{i=1}^{M} \sum_{j=1}^{N} \left| \frac{R_{ij}(t) - L_{ij}(t)}{R_{ij}(t) + L_{ij}(t)} \right|, \tag{4}$$

where M is the number of homologous channel pairs and N the frequency. The variables R_{ij} and L_{ij} represent power spectral densities (PSDs).

2.1.3 Features that quantify functional connectivity

It is assumed that neuronal oscillations and their inter-areal synchronization are essential in a normal functioning brain [43]. Oscillatory interactions between neuronal populations can be described as functional connectivity, which is the temporal correlation between neurophysiological events in different areas of the brain [44].

2.1.3.1 Magnitude squared coherence

A commonly used linear measure of functional connectivity is the magnitude squared coherence (MSC). The MSC is defined as:

$$C_{xy}(f) = \frac{|P_{xy}(f)|^2}{Pxx(f)Pyy(f)}, \tag{5}$$

with P_{xx} and P_{yy} the PSDs of signals x and y respectively and P_{xy} their cross power spectral density [25]. The MSC ranges between 0 and 1, where a MSC of 0 indicates that x and y are linearly independent and a MSC of 1 indicates that the signals are linearly dependent.

An important limitation of the MSC is that it is strongly affected by volume conduction [45]. Volume conduction describes the effects of "recording electrical potentials at a distance from their source generator" [46]. In scalp EEG there are several layers of tissue between the depolarizing neurons and

the recording electrodes. The electrodes register the electric field that is created and its transmission through the tissue. This means that an electrode not only records a signal based on the neuronal activity directly below, but that surrounding neurons also affect the signal. If the MSC is calculated for electrodes close to each other, the influence of volume conduction will be great, resulting in a high MSC [25, 45].

2.1.3.2 Weighted Phase Lag Index

In 2007 the phase lag index (PLI) was introduced by Stam at al. [47], as a reliable measure for phase synchronization. Compared to the MSC, it is not as sensitive to common sources. To determine the PLI first the phases (ϕ) of the signals of channels n are calculated as:

$$\phi_{n,t} = \arctan \frac{\tilde{x}_{n,t}}{x_{n,t}}, \tag{6}$$

where x is the signal and $\tilde{x}(t)$ its Hilbert transform [47]. Subsequently the difference in phase between the signals of two channels is calculated as:

$$\Delta\phi_{n_i,n_j,t} = \phi_{n_i,t} - \phi_{n_j,t}. \tag{7}$$

The PLI is then defined as:

$$\text{PLI} = |\mathbb{E}\{sign(\Delta\phi_{n_i,n_j,t})\}|. \tag{8}$$

Using the PLI it can be determined whether there is an asymmetry of the phase difference distribution. An asymmetry implies that there is a difference between the likelihood that the phase difference lies in the interval $-pi < \Delta\phi_{n_i,n_j,t} < 0$ and the likelihood that it lies in the interval $-pi > \Delta\phi_{n_i,n_j,t} > 0$. If there is a difference, there is a phase lag between the two signals. Symmetry of the phase difference distribution suggests that there is no coupling or the phase difference is 0 mod π. The latter can occur when a common source influences the signals.

In 2011 Vinck et al. [48] described the weighted phase lag index (WPLI) for the first time. This feature is an extension of the original PLI, with the advantages that it is not as sensitive to uncorrelated noise and has greater statistical power to identify a change in phase synchronization. The formula of the WPLI is [48]:

$$\text{WPLI} = \frac{|\mathbb{E}\{\phi_{n_i,n_j,t}\}|}{\mathbb{E}\{|\phi_{n_i,n_j,t}|\}}. \tag{9}$$

2.1.4 Features capturing complexity

The electrical activity of the brain contains complex nonlinear dynamics. Over recent years there has been increasing interest in studying the complexity of EEG signals [49]. The complexity of EEG signals can be characterized using different measures.

2.1.4.1 Sample entropy

Entropy can be described as the rate at which information is generated and quantifies the randomness and regularity of a system [50]. Many entropy algorithms have been described in the literature [51]. The sample entropy (SampEn) was introduced by Richman and Moorman [52] in 2000, as a modification of the approximate entropy (ApEn) [50]. The SampEn is the negative natural logarithm of the probability that two sequences which are similar for m data points, are also similar for $m + 1$ points. A low value of SampEn indicates a high degree of regularity and self-similarity. Advantages of the SampEn are its consistency, the fact that it is largely independent of data length and the elimination of self-matches.

When calculating the SampEn we have two input parameters: r and m, with r the tolerance and m the length of sequences to be compared. SampEn is calculated for time series of N data points: $u(1)$, $u(2)$, ..., $u(N)$. From this sequence we form the vectors $\mathbf{x}(1)$, $\mathbf{x}(2)$, ..., $\mathbf{x}(N-m+1)$, which are defined as $\mathbf{x}(i) = [u(i), u(i+1), ..., u(i+m-1)]$. We describe the distance $d[\mathbf{x}(i), \mathbf{x}(j)]$ between vectors $\mathbf{x}(i)$ and $\mathbf{x}(j)$ using the following formula, where self-matches are excluded:

$$d[\mathbf{x}(i), \mathbf{x}(j)] = \max_{k=1,2,...,m} (|u(i+k-1) - u(j+k-1)|) \text{ with } i \neq j. \tag{10}$$

Next, for every i we define C_i^m as:

$$C_i^m(r) = (\text{number of } j \text{ such that } d[\mathbf{x}(i), \mathbf{x}(j)] \leq r)/(N-m+1), \tag{11}$$

which is the probability a vector $\mathbf{x}_m(i)$ is within a distance r of $\mathbf{x}_m(j)$. Subsequently $B^m(r)$ and $A^m(r)$ are calculated, as the sum of all matches using m and $m+1$ respectively:

$$B^m(r) = (N-m)^{-1} \sum_{i=1}^{N-m} C_i^m(r), \tag{12}$$

$$A^m(r) = (N-m)^{-1} \sum_{i=1}^{N-m} C_i^{m+1}(r). \tag{13}$$

We then divide $A^m(r)$ by $B^m(r)$ and take the negative natural logarithm to determine the SampEn of the signal:

$$\text{SampEn}(r, m, N) = -\ln \frac{A^m(r)}{B^m(r)}. \tag{14}$$

2.1.4.2 Higuchi's fractal dimension

The complexity of a signal in the time domain can be quantified with the Higuchi's fractal dimension (HFD). The HFD was introduced in 1988 by Higuchi [53] as a nonlinear measure for the changing magnetic field of earth. Since then it has been applied in many different areas of science and engineering, including the analysis of physiological signals [54]. The HFD has lower computational cost than entropy-based algorithms such as the SampEn [41].

To calculate the HFD we first define a time series $x(1)$, $x(2)$, ..., $x(N)$, from which we form k new sets of time series:

$$x_k^m : x(m), x(m+k), x(m+2k), ..., x\left(m + \left[\frac{N-m}{k}\right] \cdot k\right) \text{ with } (m = 1, 2, ..., k),$$

with m the initial time, k the interval time and N the length of the original time series. The length of curve x_k^m is defines as:

$$L_m(k) = \left\{ \left(\sum_{i=1}^{[\frac{N-m}{k}]} |x(m+ik) - x(m+(i-1)\cdot k)| \right) \frac{N-1}{\left[\frac{N-m}{k}\right] \cdot k} \right\} \Big/ k. \tag{15}$$

In this formula $\frac{N-1}{\left[\frac{N-m}{k}\right] \cdot k}$ represents a normalization factor.

The mean length $L(k)$ can be determined by averaging $L_m(k)$ for all m:

$$L(k) = \frac{\sum_{m-1}^{k} L_m(k)}{k}. \tag{16}$$

The HFD can be estimated as the slope of least squares linear regression line through the points (ln(1/k), ln(L(k))).

2.1.5 Features that describe the shape of the probability distribution

All values of an EEG signal can be captured in a probability distribution. The shape of this distribution can be described by measures such as kurtosis and skewness. When calculating these measures we need to determine the second, third and fourth moment of the signal. The r^{th} central moment of a time series of length n can be calculated using the following formula [55]:

$$m_r = \frac{1}{n}\sum_{i=1}^{n}(x_i - \bar{x})^r. \tag{17}$$

2.1.5.1 Skewness

Skewness is used to describe the asymmetry of a probability distribution and is calculated using [55]:

$$\text{skewness} = \frac{m_3}{{m_2}^{3/2}}. \tag{18}$$

2.1.5.2 Kurtosis

Kurtosis provides information on the shape of the peak and tails of a probability distribution. It is calculated by [55]:

$$\text{kurtosis} = \frac{m_4}{{m_2}^{2}}. \tag{19}$$

3 Methods

3.1 Study population

Recordings with a subhairline EEG setup were performed from February 2022 until July 2022 in patients who were admitted to the emergency department (ED) of Amsterdam University Medical Centers (UMC), location AMC, with a suspected or confirmed AIS. Additional inclusion criteria were an age of 18 years or older and an onset of symptoms less than 24 hours before the EEG acquisition. The exclusion criteria were an open head wound, an active infection of the scalp or a suspected COVID-19 infection.

The study population of the current study was not attained by consecutive sampling. An intentional selection bias was introduced to enrich the study population with LVO-a stroke patients. This was done to enable exploration of differences between patients with and without LVO-a stroke despite the small study population size of this study.

The study was approved by the ethical review board of Amsterdam UMC (METC 2018_175). All included patients or their legal representatives provided written informed consent. Because the research was carried out in an emergency setting, consent was asked after EEG acquisition, as soon as logistically feasible.

3.2 Subhairline EEG setup

The subhairline EEG setup consists of wet self-adhesive electrodes (Neuroline 720, Ambu, Ballerup, Denmark). Electrodes were placed on the following electrode positions: AFpz, AF3, AF4, AFF7h, AFF8h, FFT9h, FFT10h, TPP9h and TPP10h (Figure 1). These positions belong to the 10-10 or 10-5 systems as described in [56] and correspond with locations just below the hairline. In total seven

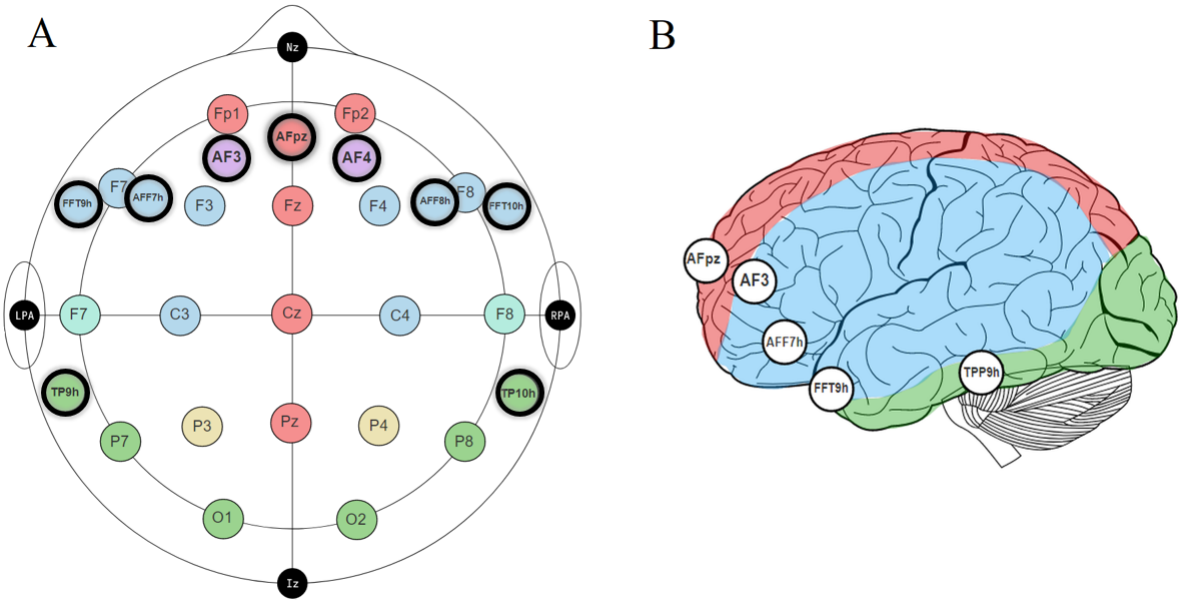

Figure 1: An overview of the electrode lay-out of the subhairline EEG setup. A: electrode positions of the international 10-20 system (circles with thin outline), together with the electrodes positions used in the subhairline EEG setup (circles with thick outline); B: approximate locations of the electrodes projected on the brain [56–59]. The vascular territories of the anterior, middle and posterior cerebral arteries are highlighted in red, blue and green, respectively [60]. This figure is an adapted version of [61].

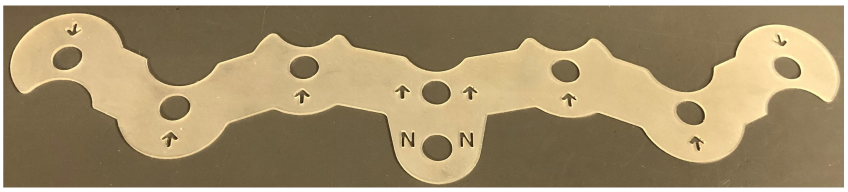

(a) The template used for reproducible placement of the electrodes. This guide is produced in sizes small, medium and large and ensures the forehead electrodes are always placed on the correct locations of the 10-10 and 10-5 systems.

(b) The self-adhesive electrodes that were used for this study (Neuroline 720, Ambu, Ballerup, Denmark).

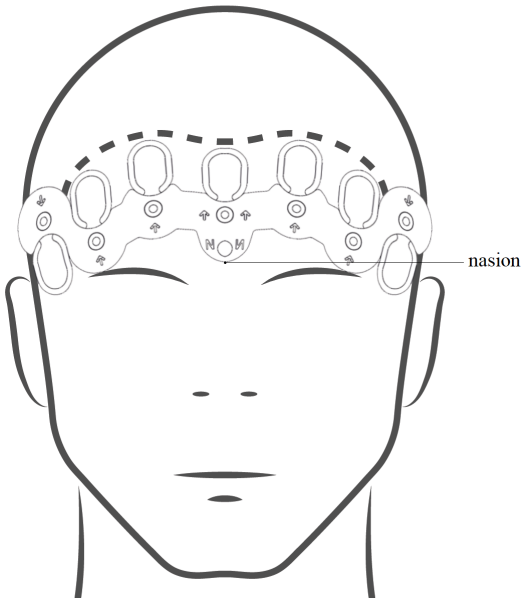

(c) An illustration of the placement of the template and electrodes on the forehead. The underside of the template is placed at the nasion. In the eight holes in the template, the studs of the electrodes can be placed. Arrows on the template indicate in what direction the electrodes need to point.

Figure 2: Components of the subhairline EEG setup.

electrodes were placed on the forehead and two were be placed behind the ears. Additionally, a ground electrode was placed right above the nasion. For all electrodes placed on the forehead, we developed a template together with the department of Medical-Technical Innovation and Development of the Amsterdam UMC, location AMC. This template was used for swift and reproducible electrode placement (Figure 2).

All electrodes were connected to an amplifier (Refa, TMSi, Oldenzaal, The Netherlands). This is an average reference amplifier, with a sample frequency set at 2048 Hz and a built-in impedance measurement function. The electrode cables were actively shielded, minimizing disturbance by external electromagnetic signals on the EEG recordings. The acquired data was accessed real-time through an application programming interface (API) created by TMSi. MATLAB R2021b (MathWorks, Natick, Massachusetts, United States) was used to connect to this API and subsequently acquire the data.

3.3 Data acquisition

With the subhairline EEG setup an EEG recording was performed in every patient as soon as logistically possible after ED admission. Before placing the electrodes, the skin was cleaned with an alcohol wipe and before starting the EEG recording the impedance level for each electrode position was measured. We aimed to reach impedance levels below 10 kOhm [62]. During the recording the patient was instructed to lie still and not talk, to prevent artifacts in the EEG data. If possible, the patients were additionally instructed to keep their eyes closed during the first half of the recording and keep them open during the second half. The intended recording duration was three minutes.

3.4 Definition of terms

In this study an LVO-a was defined as an occlusion of the first segment of the middle cerebral artery (M1), the proximal part of the second segment of the middle cerebral artery (proximal M2), the first segment of the anterior cerebral artery (A1) or the intracranial part of the internal carotid artery. Furthermore, the time of stroke onset was defined as the time the symptoms were first witnessed or, if this was unknown, the time that the patient was last-seen-well. The delta, theta, alpha and lower beta band were defined as the following respective frequency ranges: 1-4 Hz, 4-8 Hz, 8-12 Hz, 12-18 Hz. Lastly, for ROC analysis the optimal cut-off at which the sensitivity, specificity, positive predictive value (PPV) and negative predictive value (NPV) were calculated, was defined as the maximum sensitivity at a specificity of $\geq 80\%$ for LVO-a stroke.

3.5 Data analysis

The acquired EEG data was re-referenced to the following bipolar derivations of the left hemisphere: TPP9h–FFT9h, FFT9h–AFF7h, AFF7h–AF3, AF3–AFpz, FFT9h–AF3, AFF7h–AFpz, and of the right hemisphere: TPP10h–FFT10h, FFT10h–AFF8h, AFF8h–AF4, AF4–AFpz, FFT10h–AF4, AFF8h–AFpz. The bipolar signals were subsequently filtered with a third order high-pass Butterworth filter with a cut-off frequency of 0.5 Hz and third order low-pass Butterworth filter with a cut-off frequency of 35 Hz. This step was followed by artifact correction and detection.

3.5.1 Artifact correction and detection

Since most electrodes of the subhairline EEG setup were placed on the forehead, the obtained EEG signals are likely contaminated by ocular artifacts. After filtering of the signals, ocular artifacts were corrected by combining independent component analysis (ICA) with wavelet decomposition, as described by Castellanos and Makarov [63]. Wavelet enhanced ICA (wICA) ocular artifact correction was executed on the 12 bipolar EEG signals $\{x_1(t), x_2(t), ..., x_{12}(t)\}$ as follows:

1. Infomax ICA decomposition [64] of the EEG signals. We obtain mixing matrix A and 12 independent components $\{s_1(t), s_2(t), ..., s_{12}(t)\}$.
2. Multilevel wavelet decomposition using a Sym2 wavelet function and a decomposition level of 8. We obtain the detail coefficients $\{cD_8, cD_7, ..., cD_1\}$.
3. Threshold the detail coefficients by setting $cD_i(j) = 0$ when $|cD_i(j)| > K$ at index j.
4. Multilevel wavelet recomposition of the thresholded detail coefficients. We obtain $\{\tilde{s}_1(t), \tilde{s}_2(t), ..., \tilde{s}_{12}(t)\}$.
5. Compose the wICA-corrected EEG signals $\tilde{X}(t) = A \cdot [\tilde{s}_1(t), \tilde{s}_2(t), ..., \tilde{s}_{12}(t)]^T$

The threshold described by Castellanos and Makarov [63] was used: $K = \sqrt{2logN}\sigma$, where N is the length of the signals and $\sigma^2 = median(|cD_i|)/0.6745$. Furthermore, as ICA algorithm infomax ICA was used, which was first proposed by [64] and available at `https://github.com/alvarouc/ica`. The

Table 4: The EEG features calculated from the processed EEG data.

Feature group	**EEG features**
Frequency band power	Relative delta frequency band power
	Relative theta frequency band power
	Relative alpha frequency band power
	Relative lower beta frequency band power
	Normalized DAR
	Normalized TAR
	Normalized DTABR
Frequency asymmetry	pdBSI
Functional connectivity	MSC
	WPLI
Complexity	SampEn
	HFD
Probability distribution	Skewness
	Kurtosis

infomax algorithm was chosen for its superior properties over the other popular ICA algorithms, FastICA ([65]) and SOBI (second-order blind identification, [66]) in eye blink correction [67].

After ocular artifact correction the EEG signals were split into multiple epochs (described in Section 3.5.4). For each epoch automated artifact detection was applied: if the maximum epoch value exceeded the threshold of 50 μV, the epoch was excluded from further data analysis.

3.5.2 EEG features

In Table 4 the EEG features calculated from the processed data are listed. Information on these features can be found in Chapter 2, *Background: The effect of LVO-a stroke on EEG signals*. The frequency band power, complexity and probability distribution features were calculated for the bipolar channels, whereas the frequency asymmetry and functional connectivity features were logically computed for bipolar channel pairs. The relative frequency band powers were determined in relation to the frequency range 1–18 Hz. All features, except the frequency band power features, were calculated in the delta, theta, alpha and lower beta band and for the frequency range 1—18 Hz.

The EEG features were calculated for 10-second epochs with an overlap of 5 seconds. The feature values were averaged per bipolar channel or bipolar channel pair if ≥ 5 epochs were available. The frequency band power, functional connectivity, complexity and probability distribution feature values were subsequently averaged per hemisphere (if ≥ 2 unilateral bipolar channels or channel pairs were available). The averaged feature values were then labeled as ipsilesional and contralesional in case the patient had a stroke or a transient ischemic attack (TIA). For other diagnoses, the feature values were averaged over both hemispheres in case sufficient data (≥ 2 bipolar channels or channel pairs per hemisphere) were available. The frequency asymmetry values were averaged over the whole brain if ≥ 2 bipolar channel pairs were available.

3.5.3 ROC analysis

To determine the diagnostic accuracy for LVO-a stroke a ROC analysis was performed using each EEG ipsilesional feature. The area under the ROC curve (AUC), sensitivity, specificity, PPV and NPV were subsequently computed.

3.5.4 Logistic regression model

A simple logistic regression (LR) model was developed to further investigate if a combination of EEG features would improve diagnostic accuracy. This model is based on the average ipsilesional EEG feature values, calculated as described in Section . Synthetic Minority Oversampling Technique (SMOTE) was used to upsample the average EEG feature values of the minority class (LVO-a stroke) and attain a balanced data set [68]. To avoid overfitting of the LR model a feature selection algorithm, based on recursive feature elimination and the variance inflation factor, was used to select 2 EEG features. In this algorithm, features with the lowest feature importance were first recursively eliminated based on the Leave-One-Out Cross-Validation (LOOCV) score of LR models. Second, in case more than 2 features remained, features with the highest variance inflation factor were recursively eliminated until 2 final features were selected.

LOOCV was used to evaluate the performance of LR models based on the 2 selected features. Missing values were replaced by iterative imputation. This was done separately for both classes in the train sets. Imputation on the test sets was done with iterative imputers fitted on the entire train sets. Standardization was performed on the train sets, and the scalers used for this purpose were also used to transform the test sets. While fitting the LR models to the train sets, L2 regularization was applied. Subsequently, a prediction was made on every test set. These predictions were compared to the true labels, and hence the following diagnostic accuracy measures could be determined: accuracy, sensitivity, specificity, PPV and NPV. Optimization of the hyperparameters, to achieve the highest diagnostic accuracy for LVO-a stroke, was done manually. Because of the small sample size, no external validation set could be used.

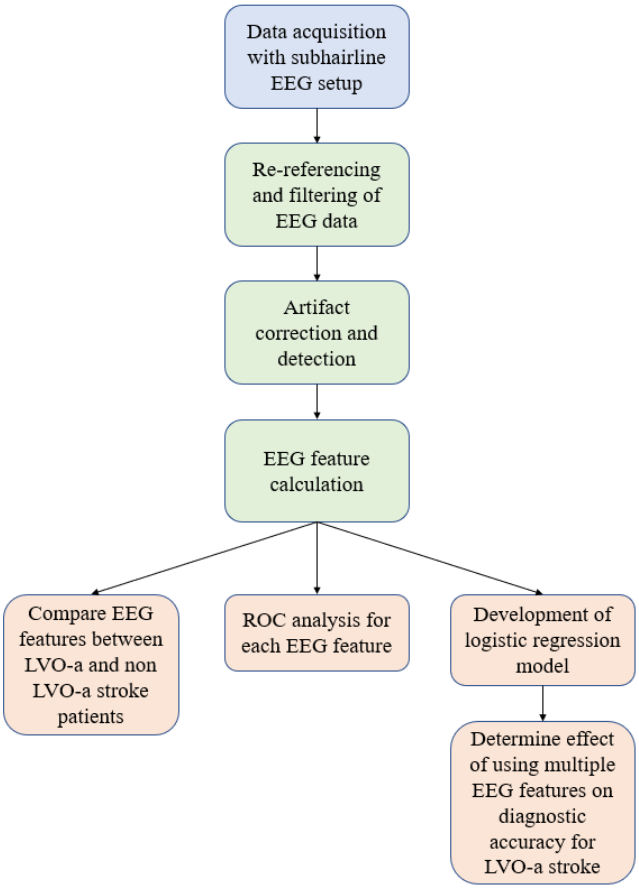

Figure 3: In this flowchart a short summary is given of the methods described in this study.

LOOCV was also used to evaluate the performance of LR models based on individual EEG features. The methods described in the paragraph above were used for these analyses. The hyperparameters were, however, not optimized manually for each EEG feature. Instead, we used the hyperparameters that were optimal for the analysis of the 2 selected EEG features.

3.5.5 Statistical analysis

The baseline characteristics of patients with and without an LVO-a stroke and their EEG feature values were compared. The independent samples t-test was used for normally distributed continuous variables, the Mann-Whitney U test was used for non-normally distributed continuous variables, and the chi-squared test (if expected count ≥ 5) or Fisher's exact test (if expected count <5) was used for categorical variables.

For all diagnostic accuracy measures, confidence intervals were calculated. For the accuracy, sensitivity, specificity, PPV and NPV the Wilson Score confidence interval was used [69]. This metric is reliable for small sample sizes and does not rely on a normal distribution. For the AUC, the confidence interval as described by Hanley and McNeil was used [70].

All data were analyzed using Python 3.8.8 (Python Software Foundation, Wilmington, Delaware, United States). A flowchart of the methods of the current study is shown in Figure 3.

4 Results

For this study an EEG recording was initiated in 42 patients. In total 5/42 (12%) patients were excluded, because deferred informed consent was not provided. Baseline characteristics of the 37 included patients are reported in Table 5. Median age of the included patients was 75 (IQR 66–81) years and 17/37 (46%) patients were female. Among the 37 patients, 13/37 (35%) had an LVO-a stroke, 14/37 (38%) a non-LVO-a ischemic stroke, 4/37 (11%) a transient ischemic attack, 2/37 (5%) a seizure, 1/37 (3%) an intracranial tumor and 3/37 (8%) another stroke mimic. Of the 13 LVO-a stroke patients, 12/13 (92%) had an M1 occlusion and 1/13 (8%) an intracranial internal carotid artery occlusion. Of the 14 non-LVO-a ischemic stroke patients 6/14 (43%) had an ischemic stroke of the anterior circulation and 8/14 (57%) had an ischemic stroke of the posterior circulation. LVO-a stroke patients were more often female than patients without an LVO-a stroke (69% vs 33%, p=0.08). The neurological deficits of patients with an LVO-a stroke were more severe compared to the patients without an LVO-a stroke (median NIHSS 16 vs 2, p<0.01). More LVO-a stroke patients were transferred from a primary stroke center than non-LVO-a stroke patients (77% vs 29%, p=0.01). There was nonetheless no statistically significant difference in median onset-to-EEG-time between the groups (344 minutes vs 242 minutes, p=0.46). Lastly, intravenous thrombolysis (IVT) was initiated prior to the EEG recording in 3/13 (23%) LVO-a stroke patients and in 5/24 (21%) patients without an LVO-a stroke (p=1.00).

A report on the impedance levels measured before each EEG recording is given in Appendix 1.

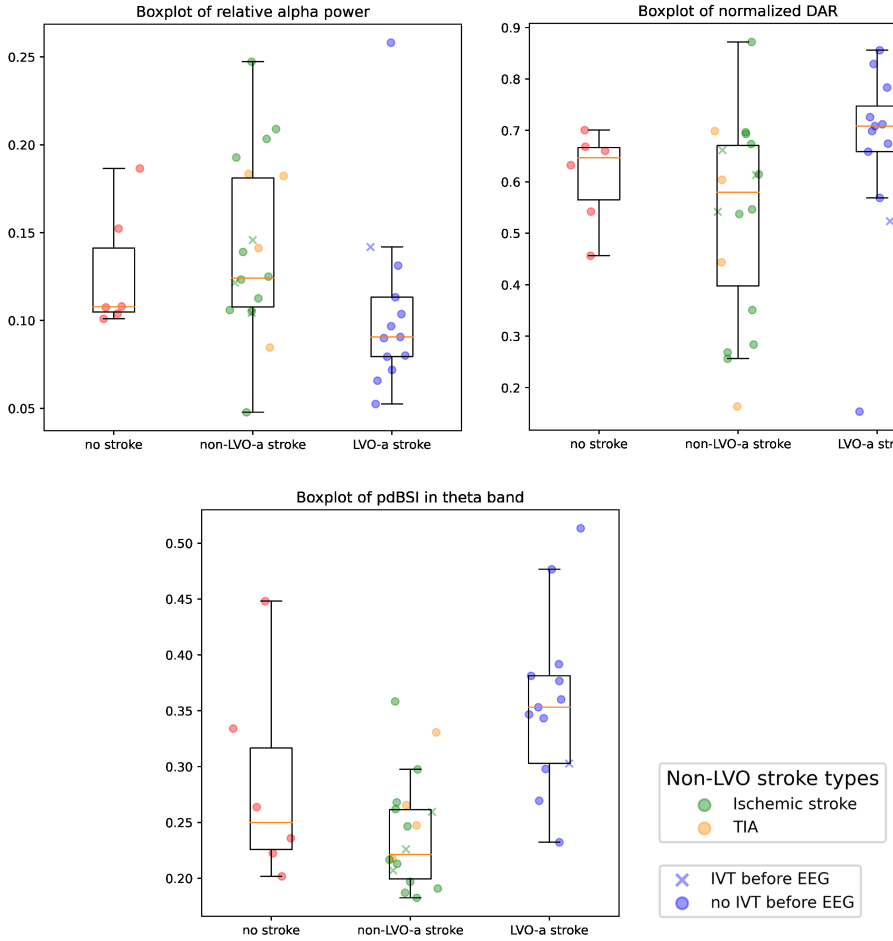

Figure 4: Boxplots of the relative alpha power, normalized DAR and pdBSI in the theta frequency band. The average feature values are shown for patients without a stroke, with a non-LVO-a stroke and with an LVO-a stroke.

Table 5: Baseline characteristics.

	All patients (n=37)	**LVO-a stroke (n=13)**	**Non-LVO-a stroke (n=24)**	***p*-values**[1]
Age, median (IQR)	75 (66–81)	75 (69–80)	74 (61–81)	0.65
Sex, no. of females/total (%)	17 (46%)	9 (69%)	8 (33%)	0.08
Medical history, no./total (%)				
Ischemic stroke	9 (24%)	2 (15%)	7 (29%)	0.45
Hemorrhagic stroke	1 (3%)	0 (0%)	1 (4%)	1.00
Intracranial tumor	1 (3%)	0 (0%)	1 (4%)	1.00
NIHSS, median (IQR)	5 (1–16)	16 (15–19)	2 (1–6)	<0.01
Transferred from PSC, no./total (%)	17 (46%)	10 (77%)	7 (29%)	0.01
Diagnosis, no./total (%)				
Ischemic stroke	27 (73%)	13 (100%)	14 (58%)	<0.01
Occlusion location[2]				
Intracranial internal carotid artery	1	1		-
M1	12	12	-	-
Distal M2	1	-	1	-
M3	1	-	1	-
A2	1	-	1	-
P2	2	-	2	-
Basilar artery	1	-	1	-
TIA	4 (11%)	0 (0%)	4 (17%)	0.28
Epilepsy	2 (5%)	0 (0%)	2 (8%)	1.00
Intracranial tumor	1 (3%)	0 (0%)	1 (4%)	1.00
Other	3 (8%)	0 (0%)	3 (13%)	0.54
Treatment, no./total (%)				
EVT	10 (27%)	9 (69%)	1 (4%)	<0.01
IVT	10 (27%)	4 (31%)	6 (25%)	0.72
Prior to EEG recording	8 (22%)	3 (23%)	5 (21%)	1.00
Timeline in minutes, median (IQR)				
Symptom onset to start EEG	250 (127–528)	344 (113–816)	242 (121–441)	0.46
ED arrival to start EEG	37 (28–47)	41 (15–49)	36 (30–43)	0.86
Start electrode application to start EEG	6 (5–6)	5 (4–6)	6 (5–7)	0.57
IVT to start EEG[3]	21 (17–82)	21 (19–54)	21 (17–80)	0.68
EEG recording duration in seconds, median (IQR)	185 (181–189)	184 (175–211)	186 (182–188)	0.80
Impedance values in kOhm, median (IQR)[4]	9 (4–20)	12 (5–25)	8 (4–15)	<0.01

A2 = second segment of the anterior cerebral artery; EEG = electroencephalography; ED = emergency department; EVT = endovascular thrombectomy; IQR = interquartile range; IVT = intravenous thrombolysis; LVO-a = anterior circulation large vessel occlusion; M1 = first segment of the middle cerebral artery; M2 = second segment of the middle cerebral artery; M3= third segment of the middle cerebral artery; NIHSS = National Institutes of Health Stroke Scale; no. = number; PSC = Primary Stroke Center; P2 = second segment of the posterior cerebral artery; TIA = transient ischemic attack.

[1] *p*-value for the difference between patients with and without an LVO-a stroke.

[2] only occlusion locations that were visible on Computed Tomography Angiography images are presented.

[3] only calculated for patients who received IVT prior to the EEG recording.

[4] based on the mean impedance values per patient.

Table 6: Ipsilesional EEG feature values of patients with and without an LVO-a stroke and the p-values of the Mann-Whitney U tests used to compare the EEG feature values. In case the patient did not have an ischemic stroke or TIA, the average feature value of both hemispheres was used.

	LVO-a stroke (n=11)	**Non-LVO-a stroke (n=24)**	***p*-values**[1]
Frequency band power			
Relative delta power	0.56 (0.51 – 0.66)	0.52 (0.48 – 0.57)	0.14
Relative theta power	0.18 (0.15 – 0.20)	0.20 (0.16 – 0.25)	0.15
Relative alpha power	**0.09 (0.08 – 0.17)**	**0.12 (0.11 – 0.18)**	**0.01**
Relative lower beta power	0.14 (0.08 – 0.11)	0.12 (0.09 – 0.15)	0.77
Normalized DAR	**0.71 (0.66 – 0.75)**	**0.61 (0.45 – 0.67)**	**0.01**
Normalized TAR	0.32 (0.10 – 0.40)	0.22 (0.08 – 0.35)	0.40
Normalized DTABR	0.52 (0.31 – 0.65)	0.49 (0.36 – 0.56)	0.52
Frequency asymmetry			
pdBSI	**0.32 (0.28 – 0.36)**[2]	**0.26 (0.24 – 0.31)**[2]	**0.01**[2]
Delta	**0.31 (0.25 – 0.43)**	**0.25 (0.21 – 0.29)**	**0.02**
Theta	**0.35 (0.30 – 0.38)**	**0.24 (0.21 – 0.27)**	**<0.01**
Alpha	**0.28 (0.24 – 0.32)**	**0.24 (0.22 – 0.27)**	**0.02**
Lower beta	0.28 (0.25 – 0.39)	0.28 (0.24 – 0.33)	0.44
Functional connectivity			
MSC	0.19 (0.17 – 0.20)[2]	0.18 (0.16 – 0.19)[2]	0.48[2]
Delta	0.24 (0.18 – 0.27)	0.17 (0.16 – 0.21)	0.09
Theta	0.20 (0.18 – 0.25)	0.19 (0.16 – 0.20)	0.31
Alpha	0.18 (0.15 – 0.18)	0.18 (0.16 – 0.20)	0.41
Lower beta	0.16 (0.14 – 0.18)	0.17 (0.15 – 0.18)	0.48
WPLI	-0.061 (-0.381 – -0.005)[2]	-0.029 (-0.157 – 0.121)[2]	0.19[2]
Delta	-0.077 (-0.132 – 0.031)	0.009 (-0.079 – 0.189)	0.16
Theta	-0.154 (-0.273 – 0.049)	-0.026 (-0.026 – 0.054)	0.30
Alpha	-0.100 (-0.194 – 0.095)	0.011 (-0.193 – 0.105)	0.75
Lower beta	0.034 (-0.056 – 0.073)	0.059 (-0.045 – 0.160)	0.34
Complexity			
Sample entropy	0.256 (0.225 – 0.300)[2]	0.263 (0.239 – 0.285)[2]	0.77[2]
Delta	0.060 (0.057 – 0.062)	0.061 (0.060 – 0.064)	0.35
Theta	0.213 (0.204 – 0.216)	0.218 (0.212 – 0.225)	0.08
Alpha	0.370 (0.369 – 0.377)	0.367 (0.364 – 0.372)	0.10
Lower beta	0.499 (0.489 – 0.500)	0.491 (0.488 – 0.497)	0.16
HFD	1.0059 (1.0052 – 1.0070)[2]	1.0054 (1.0048 – 1.0066)[2]	0.48[2]
Delta	0.9933 (0.9931 – 0.9940)	0.9938 (0.9935 – 0.9940)	0.18
Theta	0.9999 (0.9998 – 1.0000)	1.0000 (0.9996 – 1.0000)	0.65
Alpha	1.0036 (1.0034 – 1.0038)	1.0036 (1.0035 – 1.0038)	0.42
Lower beta	1.0103 (1.0101 – 1.0105)	1.0102 (1.0100 – 1.0104)	0.17
Probability distribution			
Skewness	-0.0199 (-0.0530 – 0.0377)[2]	-0.0264 (-0.0542 – -0.0080)[2]	0.25[2]
Delta	-0.0169 (-0.0496 – -0.0151)	-0.0233 (-0.0696 – 0.0042)	0.77
Theta	-0.0009 (-0.0029 – <-0.0001)	-0.0011 (-0.0025 – 0.0006)	0.77
Alpha	0.0002 (-0.0001 – 0.0003)	0.0001 (-0.0001 – 0.0002)	0.69
Lower beta	-0.0001 (-0.0003 – <0.0001)	0.0001 (-0.0001 – 0.0002)	0.05
Kurtosis	0.20 (0.05 – 0.27)[2]	0.17 (0.09 – 0.28)[2]	0.86[2]
Delta	0.20 (0.09 – 0.24)	0.21 (0.06 – 0.33)	0.46
Theta	0.16 (0.05 – 0.28)	0.15 (0.05 – 0.24)	0.69
Alpha	0.09 (0.05 – 0.19)	0.09 (0.05 – 0.18)	0.99
Lower beta	0.06 (0.04 – 0.25)	0.18 (0.06 – 0.29)	0.42

EEG feature values are expressed as median (interquartile range); bold values denote statistical significance at a $p \leq 0.05$ level; DAR = delta/alpha ratio; DTABR = (delta+theta)/(alpha+lower beta) ratio; HFD = Higuchi fractal dimension; LVO-a = anterior circulation large vessel occlusion; MSC = magnitude squared coherence; pdBSI = pairwise derived Brain Symmetry Index; TAR = theta/alpha ratio; WPLI = weighted phase lag index.

[1] p-value for the difference between patients with and without an LVO-a stroke.

[2] calculated for the frequency band 1–18Hz.

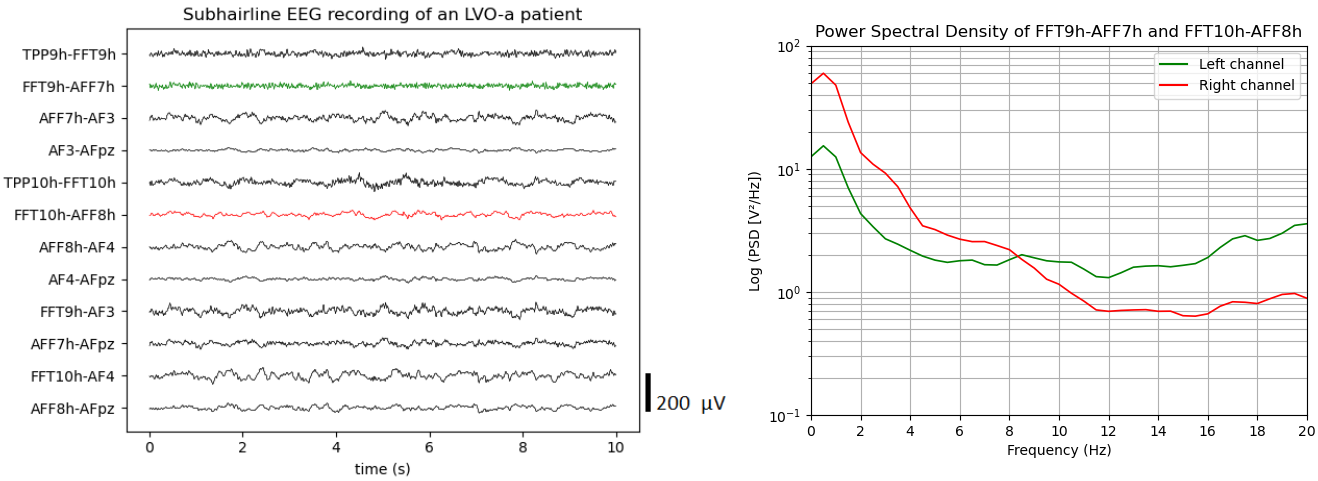

Figure 5: The subhairline EEG recording and corresponding Power Spectral Density plot of a patient with an LVO-a stroke of the right hemisphere (M1 occlusion). The Power Spectral Density plot in b) was calculated for bipolar channels FFT9h–AFF7h and FFT10h–AFF8h over 60 seconds. In a) the signals of all bipolar channels are shown for the 10 last respective seconds. In this plot the bipolar channels with even numbers are from the ipsilesional (right) hemisphere and the bipolar channels with uneven numbers from the conralesional (left) hemisphere.

4.1 Artifact correction and detection

The effects of the artifact correction and detection algorithm on EEG signals and on the results of this study are reported in Appendix 2. The algorithm satisfactorily removes ocular artifacts from the subhairline EEG signals and significantly influences EEG feature values and their diagnostic accuracy for LVO-a stroke.

4.2 EEG features

The values of all calculated ipsilesional features for LVO-a stroke patients and non-LVO-a stroke patients are shown in Table 6. All features could be calculated, except the functional connectivity features in 1/13 (8%) LVO-a stroke patient. The pdBSI was higher for LVO-a stroke patients in the delta, theta, alpha frequency band and in the frequency range 1–18 Hz (0.31 vs 0.25, p=0.02; 0.35 vs 0.24, p<0.01; 0.28 vs 0.24, p=0.02, 0.32 vs 0.26, p=0.01, respectively). The relative alpha power is lower in patients with an LVO-a stroke compared to patients without (0.09 vs 0.12, p=0.01). The DAR is higher (0.71 vs 0.61, p=0.01 for LVO-a stroke patients. No significant differences were found for the other EEG features. Boxplots of pdBSI, relative alpha and DAR values for patients without a stroke, with a non-LVO-a stroke and with an LVO-a stroke are shown in Figure 4. Moreover, as an example, the difference in PSD between the ipsilesional and contralesional hemisphere of an LVO-a stroke patient is illustrated in Figure 5. In this figure a clear asymmetry can be seen: the power in the lower frequency bands is higher for the lesioned hemisphere, whereas the power in the higher frequency bands is lower. In Appendix 3, an overview is given of the values of all contralesional features for LVO-a stroke patients and non-LVO-a stroke patients.

4.3 ROC analysis

The diagnostic measures of all ipsilesional EEG features that differed between LVO-a stroke patients and non-LVO-a stroke patients with a p-value < 0.10 are reported in Table 7. The highest diagnostic accuracy for LVO-a stroke was reached by the pdBSI in the theta frequency band (AUC=0.88; sensitivity=85%; specificity=83%; PPV=73%; NPV=91%; Figure 6). The second highest AUC was

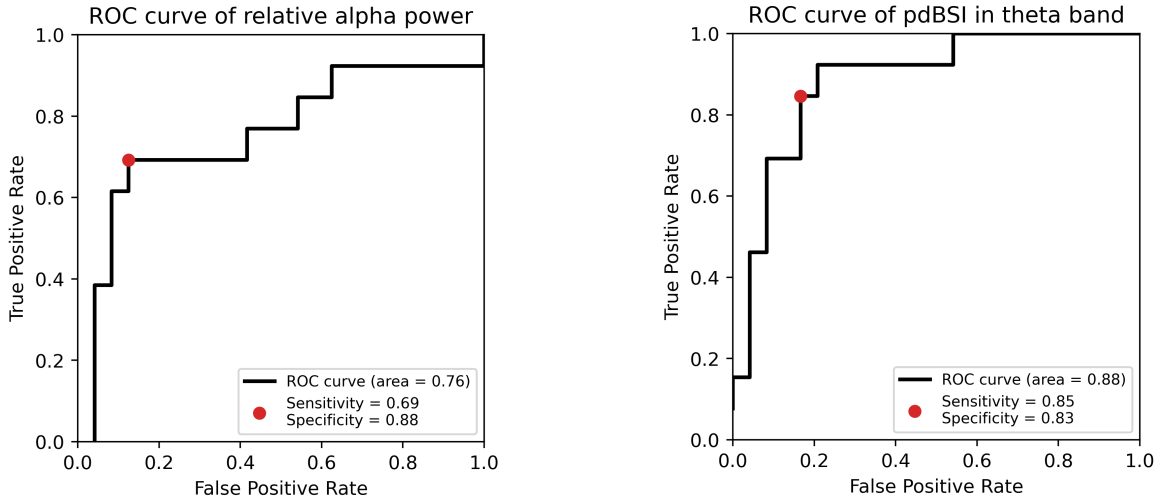

Figure 6: ROC curves of the relative alpha power and the pdBSI in the theta frequency band. The red tot indicated the optimal cut-off point, which was determined as the maximum sensitivity at a specificity of $\geq$ 80% for LVO-a stroke.

reached by the relative alpha power (AUC=0.76; sensitivity=69%; specificity=88%; PPV=75%; NPV=84%; Figure 6). The diagnostic measures of all contralesional and ipsilesional EEG features are reported in Appendix 3 and 4, respectively.

Table 7: The diagnostic accuracy for LVO-a stroke of several ipsilesional EEG features. The diagnostic accuracy is expressed as the AUC, sensitivity, specificity, PPV and NPV.

	AUC (95% CI)	**Sensitivity (95% CI)**	**Specificity (95% CI)**
Relative alpha power[a]	0.76 (0.58–0.93)	69% (42%–87%)	88% (69%–96%)
Normalized DAR[b]	0.75 (0.58–0.82)	62% (36%–82%)	88% (69%–96%)
pdBSI - 1–18Hz[c]	0.75 (0.57–0.92)	46% (23%–71%)	88% (69%–96%)
pdBSI - Delta[d]	0.73 (0.55–0.91)	46% (23%–71%)	92% (74%–98%)
pdBSI - Theta[e]	0.88 (0.76–1.00)	85% (58%–96%)	83% (64%–93%)
pdBSI - Alpha[f]	0.74 (0.56–0.92)	62% (36%–82%)	88% (69%–96%)
MSC - Delta[g]	0.68 (0.48–0.87)	50% (25%–75%)	83% (64%–93%)
SampEn - Theta[h]	0.68 (0.49–0.87)	46% (23%–71%)	92% (74%–98%)
	PPV (95% CI)	**NPV (95% CI)**	
Relative alpha power	75% (47%–91%)	84% (65%–94%)	
Normalized DAR	73% (43%–90%)	81% (62%–91%)	
pdBSI - 1–18Hz	67% (35%–88%)	75% (57%–87%)	
pdBSI - Delta	75% (41%–93%)	76% (58%–88%)	
pdBSI - Theta	73% (48%–89%)	91% (72%–97%)	
pdBSI - Alpha	73% (43%–90%)	81% (62%–91%)	
MSC - Delta	60% (31%–83%)	77% (58%–89%)	
SampEn - Theta	75% (41%–93%)	76% (58%–88%)	

AUC = area under the receiver operating characteristic curve; DAR = delta/alpha ratio; CI = confidence interval; MSC = Magnitude Squared Coherence; NPV = negative predictive value; pdBSI = pairwise derived Brain Symmetry Index; PPV = positive predictive value; SampEn = sample entropy.

LVO-a stroke was indicated at the following thresholds: [a]<0.10; [b]>0.61; [c]>0.31; [d]>0.32; [e]>0.29; [f]>0.26; [g]>0.25; [h]<0.21.

4.4 Logistic regression model

For the LR model, the feature selection algorithm selected the pdBSI in the theta frequency band and the MSC in the delta frequency band. An accuracy of 79%, sensitivity of 79%, specificity of 79%, PPV of 79% and NPV of 79% were reached using this combination of features.

An overview of the performance of all logistic regression models trained and tested using individual EEG features is given in Appendix 5. The highest diagnostic accuracy for LVO-a stroke was attained using the pdBSI in the theta frequency band (accuracy=73%; sensitivity=67%; specificity=79%; PPV=76%; NPV=70%).

5 Discussion

We studied the diagnostic accuracy of subhairline EEG for LVO-a stroke in patients with suspected stroke. The pdBSI in the theta frequency band identified LVO-a stroke patients with the highest diagnostic accuracy (AUC=0.88; sensitivity=85%; specificity=83%). The second highest diagnostic accuracy was reached by the relative alpha power (AUC=0.76; sensitivity=69%; specificity=88%). We furthermore found that diagnostic accuracy for LVO-a stroke improves when a combination of 2 EEG features is used.

5.1 Interpretation of the results

Of all EEG features, the pdBSI differed the most between patients with and without an LVO-a stroke. The pdBSI was higher in the group of LVO-a stroke patients, which implies that the spectral content of EEG signals is more asymmetric in LVO-a stroke patients. The asymmetry was strongest in the theta frequency band. This effect was also seen by Tolonen et al. (1984) [71], who studied the asymmetry of EEG features in 48 ischemic stroke patients. Frontocentrally, the theta frequency band differed the strongest between both hemispheres. While for different regions (parieto-occipital and temporal) other EEG features were more distinctive. To the best of our knowledge, the underlying pathophysiology for this location-dependent asymmetry in the theta frequency band has not been revealed.

Besides the pdBSI, the relative alpha power and the DAR differed between patients with and without an LVO-a stroke. The relative alpha power was lower and the DAR higher in LVO-a stroke patients. The same differences were observed by Van Meenen and Van Stigt et al. (2021) [20], when they compared the EEG features of 9 LVO-a stroke patients and 56 other suspected stroke patients. Finnigan et al. (2016) [19] observed similar differences between 18 AIS patients and 28 controls.

Although not statistically significant, we found a lower relative theta power and a higher relative lower beta power in LVO-a stroke patients than in non-LVO-a stroke patients. These results stand out as they are not in line with the effect of ischemic stroke on frequency band powers has been widely known and acknowledged. It has been described that reduced CBF results in a decrease in higher frequencies, followed by an increase in lower frequencies [16–19]. Van Meenen and Van Stigt et al. (2021) [20] furthermore reported that relative theta power is higher (0.63 vs 0.49, p=0.01) in LVO-a stroke patients compared to suspected stroke patients without an LVO-a stroke, using EEG data from positions FC3, FC4, CP3, CP4, FT7, FT8, TP7, and TP8. Finnigan et al. (2016) [19] compared AIS patients to healthy controls and found that relative theta power was higher (0.17 vs 0.11, p<0.0001) and relative beta power is lower (0.12 vs 0.26, p<0.0001) in AIS patients. These findings were based on EEG data from 19 electrodes covering the whole brain. Aminov et al. (2017) [72] did, on the contrary, report results that are more in line with the current study. They compared EEG recordings of 19 stroke patients and 19 healthy controls obtained at position FP1 and found lower theta power (0.28 vs 0.33, p=0.02). This suggests that the discrepancy of the current study with most existing literature could be caused because a subhairline EEG setup was used rather than an EEG setup with conventional electrode positions. The subhairline EEG setup recorded EEG signals further away from the affected area and is hence dependent on the spreading of EEG pathophysiologies. It has furthermore been suggested that theta and beta power are unreliable parameters for the evaluation of ischemic stroke [73, 74]. Theta power can be confounded by slowed alpha oscillations, and beta activity by electromyographic artifacts.

We found a diagnostic accuracy for LVO-a stroke based on ROC analysis which is comparable to the diagnostic accuracy reported in other studies that evaluated EEG for LVO-a stroke detection. Van Meenen and Van Stigt et al. (2021) [20] compared 9 LVO-a stroke patients to 56 other suspected stroke patients. With ROC analysis they reached an AUC of 0.83, sensitivity of 75% and specificity of 81% using the TAR. These values are similar to the diagnostic accuracy found in the current study using the pdBSI in the theta frequency band. Sergot et al. (2021) [22] recorded both EEG and

somatosensory-evoked potentials in 25 LVO-a stroke patients and 84 other suspected stroke patients and found a diagnostic accuracy of 80% sensitivity and 80% specificity. In contrast, Erani et al. (2020) [21] reported a lower diagnostic accuracy for LVO-a stroke in suspected stroke patients (AUC=0.69; sensitivity=41%), when using dry-electrode EEG recordings of 7 LVO-a stroke patients and 93 other suspected stroke patients. The median onset-to-EEG time was significantly longer than in the current study (564 vs 250 minutes). All patients would furthermore already have been treated for their acute symptoms, considering the median ED-arrival-to-EEG time of 222 minutes. Both elements can clarify the lower diagnostic accuracy for LVO-a stroke reported by Erani et al. (2020) [21] [75–77]

Our LR analyses have shown that a combination of 2 EEG features can increase diagnostic accuracy for LVO-a stroke. The reported diagnostic accuracy based on LR models is, however, lower than the diagnostic accuracy based on ROC analysis. During ROC analysis the entire data set is used to find the threshold at which diagnostic accuracy is optimal. The performance of our LR models was, in contrast, evaluated based on the predictions on independent test sets. This performance might furthermore not even be optimal, as hyperparameters were not automatically optimized. Both aspects explain why the LR analysis yields lower diagnostic accuracy for LVO-a stroke than ROC analysis.

In Appendix 3 we have reported on the differences in contralesional EEG features between LVO-a stroke and non-LVO-a stroke patients and on the diagnostic accuracy of these features for LVO-a stroke. The contralesional relative lower beta power and HFD in the delta frequency band differ between patients with and without an LVO-a stroke and their diagnostic accuracy is moderately high. This suggests that the contralesional hemisphere contains information which can be used to assist the detection of LVO-a stroke.

5.2 Implications of this study

Subhairline EEG has similar diagnostic accuracy for LVO-a stroke to other studies evaluating EEG for LVO-a stroke detection [20–22]. Subhairline EEG is hence a promising method for the detection of LVO-a stroke. Besides high diagnostic accuracy, main requirements for the use of subhairline EEG as triage instrument in the prehospital setting would be fast and easy application of the setup and reliable data quality in most patients.

Compared to other EEG-devices for LVO-a stroke detection [20–23] subhairline EEG has the most potential for fast and easy application. Improvements of the design of the setup and research into the use of fewer electrodes are key. An example of improved design is a forehead sticker in which all or most electrodes are integrated.

It has been shown that the quality of subhairline EEG recordings is high. In the other studies on LVO-a stroke detection using EEG, 5–35% of all EEG recordings could not be used for data analysis [20–22]. Van Meenen and Van Stigt et al. (2021) [20] stated that the patients of whom the EEG recordings were of insufficient quality more often had long hair. Subhairline EEG has the important advantage that it allows for high data quality in practically every patient, regardless of hair style.

5.3 Limitations

This study has several limitations. First of all, our main analyses were based on EEG features of the ipsilesional hemisphere. In case patients did not have an ischemic stroke or TIA, the average feature value of both hemisphere was used. We used information on the diagnosis of the patient and the localization of the lesion, which would not be available if subhairline EEG was used in a prehospital setting as triage instrument. This might have had a positive effect on the diagnostic accuracy for LVO-a stroke we reported. By averaging EEG feature values in patients without an ischemic stroke or TIA, the effect of outliers in this group is diminished. Moreover, hemispheric asymmetry that can

be caused by other conditions than an ischemic stroke or TIA, such as focal epilepsy or a tumor, is discarded by averaging over both hemispheres.

Second, the results of this study cannot be generalized to the prehospital setting. All recordings were performed in the emergency department. As a result 7 patients had already received IVT beforehand. Finnigan et al. (2006) [76] and Michaelides et al. (2010) [77] have reported that post-stroke EEG signals can significantly improve within 20 minutes after IVT administration. The fact that some patients received IVT prior to the EEG recording might have amplified differences between the EEG signals of patients with and without an LVO-a stroke. However, all LVO-a stroke patients who received IVT prior to the EEG recording were treated with EVT afterwards and at the start of EVT their occlusion was still present. We therefore expect that the IVT administration prior to the EEG recording did not affect the EEG signals of LVO-a stroke patients as much as the non-LVO-a stroke patients and this might have positively affected the diagnostic accuracy for LVO-a stroke we found.

Third, the sample size of this study is low. As a result, the confidence intervals of the diagnostic accuracy measures are broad. It is unsure whether a similar diagnostic accuracy will be reached when subhairline EEG is applied in a larger population of consecutively sampled suspected stroke patients.

Fourth, we did not adjust for multiple comparisons, as we did not want to risk a Type II statistical error (the null hypothesis is falsely accepted) in this exploratory study.

Fifth, the acquired EEG recordings are a mix of eyes-open and eyes-closed states. Research has shown that an eyes-open state is associated with a reduced EEG amplitude in the delta, theta, alpha and beta frequency bands [78, 79]. This effect exists in all areas of the brain, but is greatest in the posterior region. The mix of eyes-open and eyes-closed states could hence have affected the frequency band power features, but it is uncertain whether their diagnostic accuracy for LVO-a stroke was altered. It is furthermore unsure whether the functional connectivity, complexity and probability distribution features and their diagnostic accuracy were influenced. We do not expect the frequency asymmetry feature (pdBSI) was affected by the eyes-open and eyes-closed states, as the effects are mostly symmetrical.

Lastly, one third of all patients had a stroke or tumor in their medical history, which can cause slowing of the EEG and epileptiform activity [80–83]. Not all details on size and location of the old strokes were available, and we could hence not determine the effect on the results of the study. Medical history would, however, also affect subhairline EEG if it were to be used in the prehospital setting as triage instrument. Including patients with confounding medical history in our study thus ensures subhairline EEG is evaluated in a representational study population.

5.4 Recommendations

Before subhairline EEG could be used as triage instrument in the prehospital setting, validation in a larger consecutive prehospital study population is recommended. Furthermore, improvements are needed to make subhairline EEG feasible in the ambulance. We recommend investigating whether fewer electrodes result in the same diagnostic accuracy for LVO-a stroke and what the effect of eyes-open and eyes-closed states are on EEG feature values and diagnostic accuracy for LVO-a stroke. We would moreover advise the development of an LVO-a stroke detection algorithm based on an artificial intelligence model that combines the EEG data points with patient characteristics (e.g., the Rapid Arterial oCclusion Evaluation [RACE] scale). Adding patient characteristics is likely to improve the diagnostic accuracy of subhairline EEG for LVO-a stroke detection [21].

6 Conclusion

Subhairline EEG is a promising method for the detection of LVO-a stroke. A moderately high diagnostic accuracy for LVO-a stroke was reached using an EEG feature based on frequency asymmetry: the pdBSI. This diagnostic accuracy is similar to the diagnostic accuracy of dry electrode EEG for LVO-a stroke. In the future, validation in a larger study population and the prehospital setting is necessary.

References

[1] M. Katan and A. Luft, "Global burden of stroke," *Seminars in Neurology*, vol. 38, no. 2, pp. 208–211, 2018.

[2] GBD 2016 Stroke Collaborators, "Global, regional, and national burden of stroke, 1990–2016: a systematic analysis for the Global Burden of Disease Study 2016," *The Lancet Neurology*, vol. 18, no. 5, pp. 439–458, 2019.

[3] S. S. Virani, A. Alonso, E. J. Benjamin, M. S. Bittencourt, C. W. Callaway, *et al.*, "Heart Disease and Stroke Statistics-2020 Update: A Report From the American Heart Association," *Circulation*, vol. 141, no. 9, e139–e596, 2020.

[4] C. J. L. Murray *et al.*, "Disability-adjusted life years (DALYs) for 291 diseases and injuries in 21 regions, 1990–2010: a systematic analysis for the Global Burden of Disease Study 2010," *The Lancet*, vol. 380, no. 9859, pp. 2197–2223, 2012.

[5] V. L. Feigin *et al.*, "Update on the global burden of ischemic and hemorrhagic stroke in 1990-2013: The GBD 2013 study," *Neuroepidemiology*, vol. 45, no. 3, pp. 161–176, 2015.

[6] M. Waqas *et al.*, "Large vessel occlusion in acute ischemic stroke patients: A dual-center estimate based on a broad definition of occlusion site," *Journal of Stroke and Cerebrovascular Diseases*, vol. 29, no. 2, p. 104 504, 2020.

[7] A. Dozois *et al.*, "PLUMBER study (prevalence of large vessel occlusion strokes in Mecklenburg county emergency response)," *Stroke*, vol. 48, no. 12, pp. 3397–3399, 2017.

[8] HERMES collaborators, "Endovascular thrombectomy after large-vessel ischaemic stroke: a meta-analysis of individual patient data from five randomised trials," *The Lancet*, vol. 387, no. 10029, pp. 1723–1731, 2016.

[9] M. T. Froehler, J. L. Saver, O. O. Zaidat, R. Jahan, M. A. Aziz-Sultan, *et al.*, "Interhospital transfer before thrombectomy is associated with delayed treatment and worse outcome in the STRATIS registry (systematic evaluation of patients treated with neurothrombectomy devices for acute ischemic stroke)," *Circulation*, vol. 136, no. 24, pp. 2311–2321, 2017.

[10] E. Venema, A. E. Groot, H. F. Lingsma, W. Hinsenveld, *et al.*, "Effect of interhospital transfer on endovascular treatment for acute ischemic stroke," *Stroke*, vol. 50, no. 4, pp. 923–930, 2019.

[11] L. Pallesen *et al.*, "Safety of inter-hospital transfer of patients with acute ischemic stroke for evaluation of endovascular thrombectomy," *Scientific Reports*, vol. 10, no. 1, p. 5655, 2020.

[12] J. K. Holodinsky *et al.*, "Drip and ship versus direct to endovascular thrombectomy: The impact of treatment times on transport decision-making," *European Stroke Journal*, vol. 3, no. 2, pp. 126–135, 2018.

[13] L. S. Edwards *et al.*, "Impact of interhospital transfer on patients undergoing endovascular thrombectomy for acute ischaemic stroke in an Australian setting," *BMJ Neurology Open*, vol. 2, no. 1, 2020.

[14] C. A. Taschner *et al.*, "Drip-and-ship for thrombectomy treatment in patients with acute ischemic stroke leads to inferior clinical outcomes in a stroke network covering vast rural areas compared to direct admission to a comprehensive stroke center," *Frontiers in Neurology*, vol. 12, p. 743 151, 2021.

[15] M. V. Jayaraman *et al.*, "Field triage for endovascular stroke therapy: a population-based comparison," *Journal of NeuroInterventional Surgery*, vol. 12, no. 3, pp. 233–239, 2020.

[16] M. J. A. M. van Putten and J. Hofmeijer, "EEG monitoring in cerebral ischemia: Basic concepts and clinical applications," *Journal of Clinical Neurophysiology*, vol. 33, no. 3, pp. 203–210, 2016.

[17] B. Foreman and J. Claassen, "Quantitative EEG for the detection of brain ischemia," *Critical Care*, vol. 16, no. 2, p. 216, 2012.

[18] J. Wu, R. Srinivasan, E. Burke Quinlan, A. Solodkin, S. L. Small, and S. C. Cramer, "Utility of EEG measures of brain function in patients with acute stroke," *Journal of Neurophysiology*, vol. 115, no. 5, pp. 2399–2405, 2016.

[19] S. Finnigan, A. Wong, and S. Read, "Defining abnormal slow EEG activity in acute ischaemic stroke: Delta/alpha ratio as an optimal QEEG index," *Clinical Neurophysiology*, vol. 127, no. 2, pp. 1452–1459, 2016.

[20] L. C. C. van Meenen *et al.*, "Detection of large vessel occlusion stroke with electroencephalography in the emergency room: first results of the ELECTRA-STROKE study," *Journal of Neurology*, vol. 269, no. 4, pp. 2030–2038, 2021.

[21] F. Erani *et al.*, "Electroencephalography might improve diagnosis of acute stroke and large vessel occlusion," *Stroke*, vol. 51, no. 11, pp. 3361–3365, 2020.

[22] P. B. Sergot *et al.*, "Portable neuromonitoring device detects large vessel occlusion in suspected acute ischemic stroke," *Stroke*, vol. 52, no. 4, pp. 1437–1440, 2021.

[23] L. Shreve *et al.*, "Electroencephalography measures are useful for identifying large acute ischemic stroke in the emergency department," *Journal of Stroke and Cerebrovascular Diseases*, vol. 28, no. 8, pp. 2280–2286, 2019.

[24] R. V. A. Sheorajpanday, G. Nagels, A. J. T. M. Weeren, M. J. A. M. van Putten, and P. P. De Deyn, "Reproducibility and clinical relevance of quantitative EEG parameters in cerebral ischemia: A basic approach," *Clinical Neurophysiology*, vol. 120, no. 5, pp. 845–855, 2009.

[25] R. C. Van Kaam, M. van Putten, S. E. Vermeer, and J. Hofmeijer, "Contralesional brain activity in acute ischemic stroke," *Cerebrovascular Diseases*, vol. 45, pp. 85–92, 2018.

[26] H. Hinrichs, M. Scholz, A. K. Baum, J. W. Y. Kam, R. T. Knight, and H. Heinze, "Comparison between a wireless dry electrode EEG system with a conventional wired wet electrode EEG system for clinical applications," *Scientific Reports*, vol. 10, no. 1, p. 5218, 2020.

[27] S. Finnigan and A. Wong, "Towards pre-hospital identification of acute ischemic stroke: The value of QEEG from a single frontal channel," *Clinical Neurophysiology*, vol. 131, no. 8, pp. 1726–1727, 2020.

[28] I. Hussain and S. J. Park, "HealthSOS: Real-time health monitoring system for stroke prognostics," *IEEE Access*, vol. 8, pp. 213 574–213 586, 2020.

[29] M. Gottlibe *et al.*, "Stroke identification using a portable EEG device – A pilot study," *Neurophysiologie Clinique*, vol. 50, no. 1, pp. 21–25, 2020.

[30] C. M. Wilkinson, J. I. Burrell, J. W. P. Kuziek, S. Thirunavukkarasu, B. H. Buck, and K. E. Mathewson, "Predicting stroke severity with a 3-min recording from the Muse portable EEG system for rapid diagnosis of stroke," *Scientific Reports*, vol. 10, no. 1, p. 18 465, 2020.

[31] G. Rabiller, J. He, Y. Nishijima, A. Wong, and J. Liu, "Perturbation of brain oscillations after ischemic stroke: A potential biomarker for post-stroke function and therapy," *International Journal of Molecular Sciences*, vol. 16, no. 10, pp. 25 605–25 640, 2015.

[32] J. Astrup, B. K. Siesjö, and L. Symon, "Thresholds in cerebral ischemia - the ischemic penumbra," *Stroke*, vol. 12, no. 6, pp. 723–725, 1981.

[33] K. G. Jordan, "Emergency EEG and continuous EEG monitoring in acute ischemic stroke," *Journal of Clinical Neurophysiology*, vol. 21, no. 5, pp. 341–352, 2004.

[34] K. A. Hossmann, "Viability thresholds and the penumbra of focal ischemia," *Annals of Neurology*, vol. 36, no. 4, pp. 557–565, 1994.

[35] F. W. Sharbrough, J. M. J. Messick, and T. M. J. Sundt, "Correlation of continuous electroencephalograms with cerebral blood flow measurements during carotid endarterectomy," *Stroke*, vol. 4, no. 4, pp. 674–683, 1973.

[36] E. Faught, "Current role of electroencephalography in cerebral ischemia," *Stroke*, vol. 24, no. 4, pp. 609–613, 1993.

[37] H. Bolay, Y. Gürsoy-Özdemir, Y. Sara, R. Onur, A. Can, and T. Dalkara, "Persistent defect in transmitter release and synapsin phosphorylation in cerebral cortex after transient moderate ischemic injury," *Stroke*, vol. 33, no. 5, pp. 1369–1375, 2002.

[38] J. le Feber, S. Tzafi Pavlidou, N. Erkamp, M. J. A. M. van Putten, and J. Hofmeijer, "Progression of neuronal damage in an in vitro model of the ischemic penumbra," *PLOS ONE*, vol. 11, no. 2, pp. 1–19, 2016.

[39] C. D. Brisson, Y.-T. Hsieh, D. Kim, A. Y. Jin, and R. D. Andrew, "Brainstem neurons survive the identical ischemic stress that kills higher neurons: Insight to the persistent vegetative state," *PLOS ONE*, vol. 9, no. 5, pp. 1–16, 2014.

[40] S. Liu *et al.*, "Abnormal EEG complexity and functional connectivity of brain in patients with acute thalamic ischemic stroke," *Computational and Mathematical Methods in Medicine*, vol. 2016, p. 2 582 478, 2016.

[41] M. Rubega *et al.*, "EEG fractal analysis reflects brain impairment after stroke," *Entropy*, vol. 23, no. 5, 2021.

[42] F. Zappasodi, E. Olejarczyk, L. Marzetti, G. Assenza, V. Pizzella, and F. Tecchio, "Fractal dimension of EEG activity senses neuronal impairment in acute stroke," *PLOS ONE*, vol. 9, no. 6, e100199, 2014.

[43] A. M. Bastos and J. Schoffelen, "A tutorial review of functional connectivity analysis methods and their interpretational pitfalls," *Frontiers in Systems Neuroscience*, vol. 9, no. 175, 2016.

[44] K. J. Friston, C. D. Frith, P. F. Liddle, and R. S. Frackowiak, "Functional connectivity: the principal-component analysis of large (PET) data sets," *Journal of Cerebral Blood Flow and Metabolism*, vol. 13, no. 1, pp. 5–14, 1993.

[45] R. Srinivasan, W. R. Winter, J. Ding, and P. L. Nunez, "EEG and MEG coherence: measures of functional connectivity at distinct spatial scales of neocortical dynamics," *Journal of Neuroscience Methods*, vol. 166, no. 1, pp. 41–52, 2007.

[46] S. B. Rutkove, "Introduction to volume conduction," in *The Clinical Neurophysiology Primer*, Humana Press, Totowa, New Jersey, 2007.

[47] C. J. Stam, G. Nolte, and A. Daffertshofer, "Phase lag index: assessment of functional connectivity from multi channel EEG and MEG with diminished bias from common sources," *Human Brain Mapping*, vol. 28, no. 11, pp. 1178–1193, 2007.

[48] M. Vinck, R. Oostenveld, M. van Wingerden, F. Battaglia, and C. M. A. Pennartz, "An improved index of phase-synchronization for electrophysiological data in the presence of volume-conduction, noise and sample-size bias," *NeuroImage*, vol. 55, no. 4, pp. 1548–1565, 2011.

[49] J. Sun *et al.*, "Complexity analysis of EEG, MEG, and fMRI in mild cognitive impairment and Alzheimer's disease: a Review.," *Entropy*, vol. 22, no. 2, p. 239, 2020.

[50] S. M. Pincus, "Approximate entropy as a measure of system complexity," *Proceedings of the National Academy of Sciences*, vol. 88, no. 6, pp. 2297–2301, 1991.

[51] Z. Liang *et al.*, "EEG entropy measures in anesthesia," *Frontiers in Computational Neuroscience*, vol. 9, no. 16, pp. 1–17, 2015.

[52] J. S. Richman and J. R. Moorman, "Physiological time-series analysis using approximate entropy and sample entropy," *American Journal of Physiology-Heart and Circulatory Physiology*, vol. 278, no. 6, H2039–H2049, 2000.

[53] T. Higuchi, "Approach to an irregular time series on the basis of the fractal theory," *Physica D: Nonlinear Phenomena*, vol. 31, no. 2, pp. 277–283, 1988.

[54] S. Kesić and S. Z. Spasić, "Application of Higuchi's fractal dimension from basic to clinical neurophysiology: A review," *Computer Methods and Programs in Biomedicine*, vol. 133, pp. 55–70, 2016.

[55] S. Kokoska and D. Zwillinger, *CRC Standard Probability and Statistics Tables and Formulae*, 1st ed. Chapman Hall/CRC, 2000.

[56] R. Oostenveld and P. Praamstra, "The five percent electrode system for high-resolution EEG and ERP measurements," *Clinical Neurophysiology*, vol. 112, no. 4, pp. 713–719, 2001.

[57] G. M. Rojas, C. Alvarez, C. E. Montoya, M. de la Iglesia-Vayá, J. E. Cisternas, and M. Gálvez, "Study of resting-state functional connectivity networks using EEG electrodes position as seed," *Frontiers in Neuroscience*, vol. 12, no. 235, pp. 1–12, 2018.

[58] C. M. Michel and D. Brunet, "EEG source imaging: A practical review of the analysis steps," *Frontiers in Neurology*, vol. 10, no. 325, pp. 1–18, 2019.

[59] G. H. Klem, H. O. Lüders, H. H. Jasper, and C. Elger, "The ten-twenty electrode system of the International Federation," *Electroencephalography and Clinical Neurophysiology: Supplement*, vol. 52, pp. 3–6, 1999.

[60] H. P. Amin and J. L. Schindler, "Vascular Neuroanatomy," in *Vascular Neurology Board Review: An Essential Study Guide*. Springer International Publishing, 2017, pp. 9–21.

[61] L. R. Krol, *EEG 10-10 system with additional information*, `https://commons.wikimedia.org/wiki/File:EEG_10-10_system_with_additional_information.svg`, 2020.

[62] S. R. Sinha *et al.*, "American clinical neurophysiology society guideline 1: Minimum technical requirements for performing clinical electroencephalography," *Journal of Clinical Neurophysiology*, vol. 33, no. 4, pp. 303–307, 2016.

[63] N. P. Castellanos and V. A. Makarov, "Recovering EEG brain signals: artifact suppression with wavelet enhanced independent component analysis," *Journal of Neuroscience Methods*, vol. 158, no. 2, pp. 300–312, 2006.

[64] A. J. Bell and T. J. Sejnowski, "An information-maximization approach to blind separation and blind deconvolution," *Neural Computation*, vol. 7, no. 6, pp. 1129–1159, 1995.

[65] A. Hyvärinen, "Fast and robust fixed-point algorithms for independent component analysis," *IEEE Transactions on Neural Networks*, vol. 10, no. 3, pp. 626–634, 1999.

[66] A. Belouchrani, K. Abed-Meraim, J. F. Cardoso, and E. Moulines, "A blind source separation technique using second-order statistics," *IEEE Transactions on Signal Processing*, vol. 45, no. 2, pp. 434–444, 1997.

[67] M. B. Pontifex, K. L. Gwizdala, A. C. Parks, M. Billinger, and C. Brunner, "Variability of ICA decomposition may impact EEG signals when used to remove eyeblink artifacts," *Psychophysiology*, vol. 54, no. 3, pp. 386–398, 2017.

[68] N. Chawla, K. Bowyer, L. Hall, and W. Kegelmeyer, "SMOTE: Synthetic Minority Over-sampling Technique," *Journal of Artificial Intelligence Research*, vol. 16, pp. 321–357, 2002.

[69] E. B. Wilson, "Probable inference, the law of succession, and statistical inference," *Journal of the American Statistical Association*, vol. 22, no. 158, pp. 209–212,

[70] J. A. Hanley and B. J. McNeil, "The meaning and use of the area under a receiver operating characteristic (ROC) curve," *Radiology*, vol. 143, no. 1, pp. 29–36, 1982.

[71] U. Tolonen, "Parametric relationships between four different quantitative EEG methods in cerebral infarction," Progress in Brain Research, vol. 62, pp. 51–64, 1984.

[72] A. Aminov, J. M. Rogers, S. J. Johnstone, S. Middleton, and P. H. Wilson, "Acute single channel EEG predictors of cognitive function after stroke," *PLOS ONE*, vol. 12, no. 10, e0185841, 2017.

[73] S. P. Finnigan, M. Walsh, S. E. Rose, and J. B. Chalk, "Quantitative EEG indices of sub-acute ischaemic stroke correlate with clinical outcomes," *Clinical Neurophysiology*, vol. 118, no. 11, pp. 2525–2532, 2007.

[74] M. R. Nuwer, S. E. Jordan, and S. S. Ahn, "Evaluation of stroke using EEG frequency analysis and topographic mapping," *Neurology*, vol. 37, no. 7, p. 1153, 1987.

[75] R. Brouns and P. P. De Deyn, "The complexity of neurobiological processes in acute ischemic stroke," *Clinical Neurology and Neurosurgery*, vol. 111, no. 6, pp. 483–495, 2009.

[76] S. P. Finnigan, S. E. Rose, and J. B. Chalk, "Rapid EEG changes indicate reperfusion after tissue plasminogen activator injection in acute ischaemic stroke," *Clinical Neurophysiology*, vol. 117, no. 10, pp. 2338–2339, 2006.

[77] C. Michaelides, T. N. Nguyen, K. H. Chiappa, C. J. Kwolek, and M. V. Simon, "Cerebral embolism during elective carotid endarterectomy treated with tissue plasminogen activator: utility of intraoperative EEG monitoring," *Clinical Neurology and Neurosurgery*, vol. 112, no. 5, pp. 446–449, 2010.

[78] A. S. Geller *et al.*, "Eye closure causes widespread low-frequency power increase and focal gamma attenuation in the human electrocorticogram," *Clinical Neurophysiology*, vol. 125, no. 9, pp. 1764–1773, 2014.

[79] R. J. Barry and F. M. De Blasio, "EEG differences between eyes-closed and eyes-open resting remain in healthy ageing," *Biological Psychology*, vol. 129, pp. 293–304, 2017.

[80] S. Giaquinto, A. Cobianchi, F. Macera, and G. Nolfe, "EEG recordings in the course of recovery from stroke," *Stroke*, vol. 25, no. 11, pp. 2204–2209, 1994.

[81] M. E. Wolf, A. D. Ebert, and A. Chatzikonstantinou, "The use of routine EEG in acute ischemic stroke patients without seizures: generalized but not focal EEG pathology is associated with clinical deterioration," *International Journal of Neuroscience*, vol. 127, no. 5, pp. 421–426, 2017.

[82] J. W. Doria and P. B. Forgacs, "Incidence, implications, and management of seizures following ischemic and hemorrhagic stroke," *Current Neurology and Neuroscience Reports*, vol. 19, no. 7, p. 37, 2019.

[83] S. Handayani, Y. Diansari, E. Bahar, and W. Novantina, "EEG changes in patients with intracranial tumors and seizures symptom at Mohammad Hoesin Hospital Palembang," *Journal of Physics: Conference Series*, vol. 1246, no. 1, p. 12 014, 2019.

Appendix 1: Impedance levels

Before the start of every EEG recording impedance levels were measured for all electrodes. We aimed to reach impedance levels below 10 kOhm, in line with the guidelines for performing clinical EEG [1]. This aim, however, was not always achievable, as some recordings were performed in an acute setting.

The median impedance level for all patients and every electrode position is 9 (IQR 4–20). For LVO-a stroke patients the median impedance level is 12 (IQR 5–25) and for non-LVO-a stroke patients it is 8 (IQR 4–15). There is a statistically significant difference in impedance levels between these two groups (p=0.003). This could be caused by the generally more acute settings in which the EEG recordings of LVO-a patients were performed.

In Table 8 the impedance levels for all electrode positions are reported separately. The median impedance levels and the interquartile ranges are higher for LVO-a stroke patients, but these differences are not statistically significant.

Table 8: Impedance levels for each individual electrode position.

	AFpz	**AF3**	**AF4**	**AFF7h**	**AFF8h**	**FFT9h**	**FFT10h**	**TTP9h**	**TTP10h**
All patients[1]	5 (3–10)	8 (4–15)	7 (3–13)	11 (6–31)	7 (4–24)	13 (10–23)	8 (4–15)	13 (6–31)	7 (2–24)
LVO-a stroke[1]	8 (4–14)	8 (5–21)	7 (3–22)	27 (8–32)	14 (5–37)	16 (10–25)	10 (5–26)	11 (5–31)	10 (3–30)
No LVO-a stroke[1]	4 (3–10)	6 (3–13)	6 (3–11)	10 (5–23)	6 (3–14)	12 (9–25)	5 (3–13)	19 (5–31)	6 (2–22)
p-value[2]	0.20	0.20	0.09	0.07	0.27	0.32	0.18	0.48	0.38

impedance levels are given in kOhm, median (interquartile range).
[1] 37 patients in total, 13 LVO-a stroke patients and 24 patients without an LVO-a stroke.
[2] p-value for the difference between patients with and without an LVO-a stroke.

References

[1] S. R. Sinha *et al.*, "American clinical neurophysiology society guideline 1: Minimum technical requirements for performing clinical electroencephalography," *Journal of Clinical Neurophysiology*, vol. 33, no. 4, pp. 303–307, 2016.

Appendix 2: Effect of artifact correction and detection

Background

There was a specific need to remove ocular artifacts from the signals, as most recording electrodes of the subhairline EEG setup were placed on the forehead, where the influence of ocular artifacts is great. The acquired subhairline EEG recordings in this study have hence been processed with an artifact correction and detection algorithm. This algorithm was developed to correct ocular artifacts and to determine if other large amplitude artifacts occur in the signal.

One of the most acknowledged ocular artifact correction algorithms is ICA [1]. By using ICA an artifact source can be separated from clean EEG signals. The efficacy of the algorithm is however strongly influenced by the number of available channels: the number of independent components (sources) obtained with ICA is equal to the number of EEG channels. When there are too few channels, the artifact source cannot be separated from the clean EEG successfully and will hence also contain true cerebral activity. If the independent component is removed, part of the cerebral activity in the EEG signals is lost. The performance of ICA can be enhanced in several ways. ICA can for instance be combined with wavelet decomposition, empirical mode decomposition and adaptive filtering [1]. The use of adaptive filtering is, however, not always feasible as a ocular reference signal is needed. Between wavelet and empirical mode decomposition, wavelet decomposition is most commonly used in combination with ICA and it has been shown that it performs well [1–3].

We investigated the effect of ocular artifact correction on EEG signals, the corresponding EEG features and their diagnostic accuracy for LVO-a stroke. We furthermore evaluated the effect of only applying artifact detection to the EEG signals. We hypothesized that artifact correction and detection would increase the reliability of the calculated EEG features and improve diagnostic accuracy for LVO-a stroke.

Methods

In this study ICA was combined with wavelet decomposition, as described by Castellanos and Makarov [2]. The wICA algorithm is described in detail in the main body of this thesis, Section 3.5.1. After ocular artifact correction by wICA, automated artifact detection was applied: if the maximum epoch value exceeded the threshold of 50 μV, epochs were excluded from further data analysis. We assessed the performance of the artifact correction algorithm in our data by manual inspection of the raw and

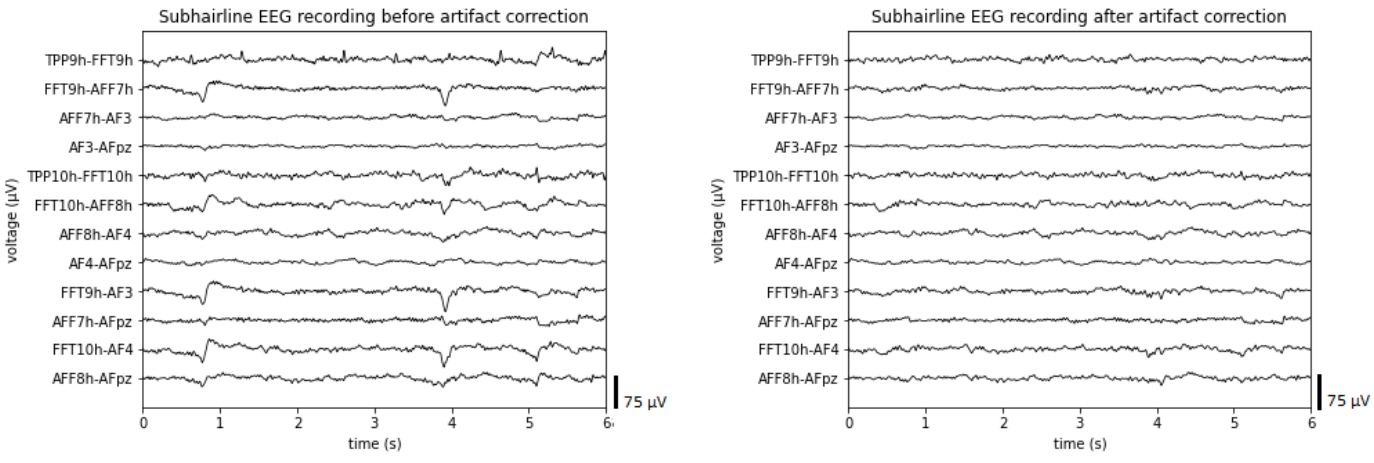

Figure 7: The effect of ocular artifact correction on all bipolar subhairline EEG signals.

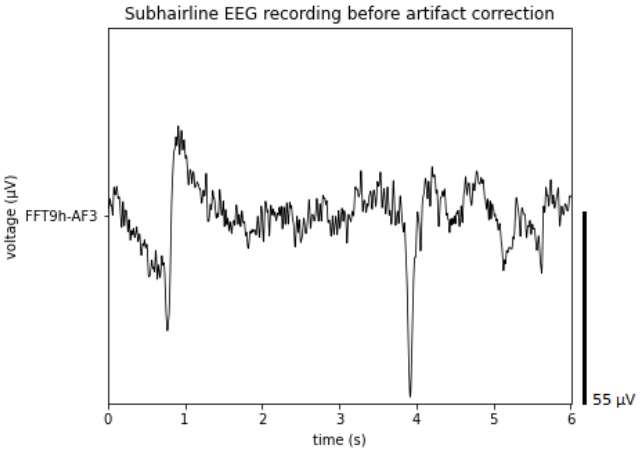

(a)

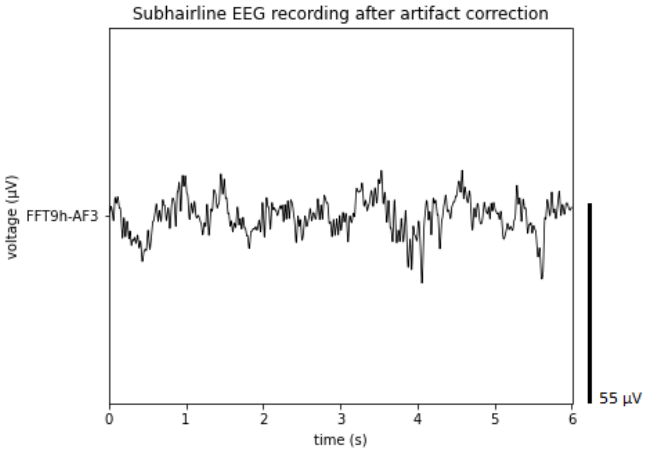

(b)

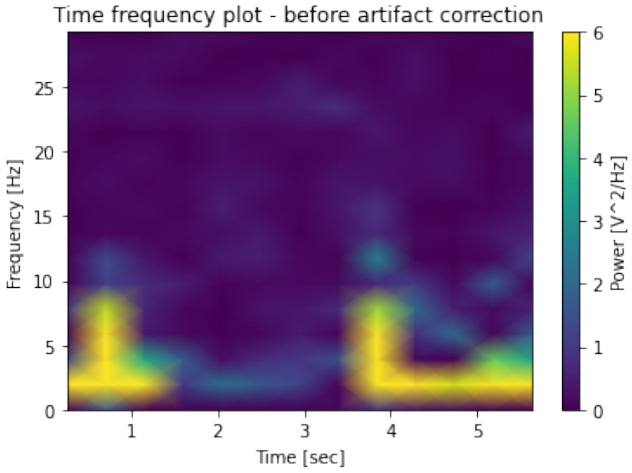

(c)

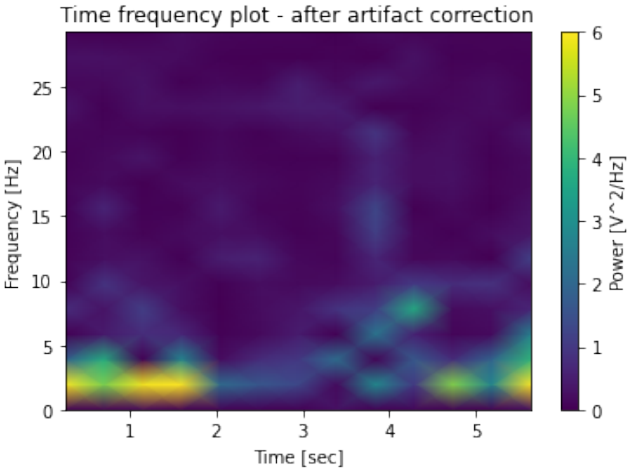

(d)

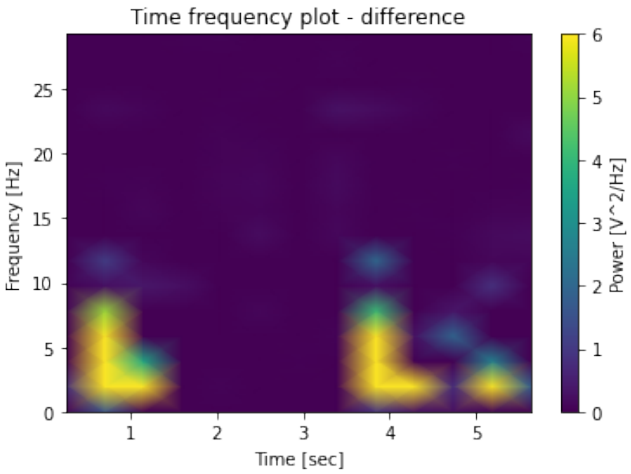

(e)

Figure 8: The effect of ocular artifact correction on a subhairline EEG signal; a) the raw EEG signal; b) the EEG signal after ocular artifact correction; c) the time frequency plot of the raw EEG signal; d) the time frequency plot of the EEG signal after ocular artifact correction; e) the difference between the time frequency plots, calculated by subtracting the plot in d) from the plot in c).

Table 9: An overview of the effect of artifact correction and detection on ipsilesional EEG feature values and the corresponding area under the ROC curve.

	LVO-a stroke (n=11)	**No LVO-a stroke (n=24)**	***p*-values**[1]	**AUC (95% CI)**
No artifact correction or detection				
RDP	0.24 (0.18 – 0.36)	0.36 (0.24 – 0.44)	0.07	0.68 (0.49 – 0.87)
RTP	0.19 (0.18 – 0.20)	0.19 (0.17 – 0.21)	0.94	0.51 (0.31 – 0.71)
RAP	0.23 (0.19 – 0.24)	0.17 (0.13 – 0.22)	0.04	0.71 (0.53 – 0.85)
RBP	0.35 (0.27 – 0.40)	0.27 (0.21 – 0.34)	0.06	0.69 (0.50 – 0.88)
nDAR	-0.10 (-0.20 – 0.23)	0.27 (-0.02 – 0.44)	0.05	0.70 (0.51 – 0.89)
nTAR	-0.05 (-0.11 – -0.01)	0.09 (-0.05 – 0.25)	0.04	0.71 (0.53 – 0.89)
nDTABR	-0.15 (-0.27 – -0.08)	0.14 (-0.11 – 0.32)	0.05	0.70 (0.52 – 0.89)
pdBSI[2]	0.39 (0.32 – 0.47)	0.34 (0.29 – 0.41)	0.21	0.63 (0.43 – 0.82)
MSC[2]	0.19 (0.18 – 0.23)	0.18 (0.17 – 0.22)	0.40	0.59 (0.39 – 0.78)
WPLI[2]	-0.02 (-0.07 – 0.08)	-0.03 (-0.13 – 0.04)	0.56	0.56 (0.36 – 0.76)
SampEn[2]	0.34 (0.31 – 0.38)	0.31 (0.28 – 0.35)	0.08	0.68 (0.49 – 0.87)
HFD[2]	1.0077 (1.0074 – 1.0081)	1.0072 (1.0062 – 1.0078)	0.05	0.70 (0.51 – 0.88)
Skewness[2]	-0.02 (-0.06 – 0.01)	-0.02 (-0.05 – <-0.01)	0.89	0.52 (0.32 – 0.71)
Kurtosis[2]	0.49 (0.22 – 1.27)	0.55 (0.30 – 0.88)	0.86	0.52 (0.32 – 0.71)
Only artifact detection				
RDP	0.22 (0.18 – 0.36)	0.36 (0.23 – 0.44)	0.07	0.69 (0.50 – 0.87)
RTP	0.19 (0.17 – 0.20)	0.19 (0.17 – 0.21)	0.79	0.53 (0.33 – 0.73)
RAP	0.23 (0.19 – 0.24)	0.17 (0.13 – 0.22)	0.04	0.73 (0.52 – 0.89)
RBP	0.35 (0.27 – 0.40)	0.28 (0.21 – 0.34)	0.05	0.70 (0.51 – 0.88)
nDAR	-0.12 (-0.19 – -0.23)	0.25 (-0.03 – 0.44)	0.04	0.71 (0.52 – 0.89)
nTAR	-0.05 (-0.11 – -0.01)	0.08 (-0.05 – 0.25)	0.04	0.71 (0.53 – 0.89)
nDTABR	-0.17 (-0.27 – 0.08)	0.12 (-0.10 – 0.32)	0.05	0.70 (0.52 – 0.89)
pdBSI[2]	0.33 (0.27 – 0.41)	0.24 (0.20 – 0.31)	0.18	0.64 (0.44 – 0.83)
MSC[2]	0.19 (0.18 – 0.24)	0.18 (0.17 – 0.22)	0.32	0.60 (0.41 – 0.80)
WPLI[2]	-0.04 (-0.09 – 0.08)	-0.03 (-0.12 – 0.05)	0.81	0.53 (0.33 – 0.72)
SampEn[2]	0.35 (0.31 – 0.38)	0.31 (0.27 – 0.35)	0.05	0.70 (0.51 – 0.88)
HFD[2]	1.0077 (1.0075 – 1.0081)	1.0072 (1.0061 – 1.0078)	0.05	0.70 (0.51 – 0.88)
Skewness[2]	-0.02 (-0.06 – 0.01)	-0.02 (-0.05 – <-0.01)	0.96	0.51 (0.31 – 0.70)
Kurtosis[2]	0.50 (0.22 – 1.14)	0.54 (0.30 – 0.90)	0.99	0.50 (0.31 – 0.70)
Artifact correction and detection				
RDP	0.56 (0.51 – 0.66)	0.52 (0.48 – 0.57)	0.14	0.65 (0.46 – 0.84)
RTP	0.18 (0.15 – 0.20)	0.20 (0.16 – 0.25)	0.15	0.65 (0.46 – 0.84)
RAP	0.09 (0.08 – 0.17)	0.12 (0.11 – 0.18)	0.01	0.76 (0.58 – 0.93)
RBP	0.14 (0.08 – 0.11)	0.12 (0.09 – 0.15)	0.77	0.53 (0.33 – 0.73)
nDAR	0.71 (0.66 – 0.75)	0.61 (0.45 – 0.67)	0.01	0.75 (0.58 – 0.82)
nTAR	0.32 (0.10 – 0.40)	0.22 (0.08 – 0.35)	0.40	0.59 (0.39 – 0.78)
nDTABR	0.52 (0.31 – 0.65)	0.49 (0.36 – 0.56)	0.52	0.57 (0.37 – 0.77)
pdBSI[2]	0.32 (0.28 – 0.36)	0.26 (0.24 – 0.31)	0.01	0.75 (0.57 – 0.92)
MSC[2]	0.19 (0.17 – 0.20)	0.18 (0.16 – 0.19)	0.48	0.58 (0.37 – 0.78)
WPLI[2]	-0.06 (-0.38 – -0.01)	-0.03 (-0.16 – 0.12)	0.19	0.64 (0.44 – 0.84)
SampEn[2]	0.26 (0.23 – 0.30)	0.26 (0.24 – 0.29)	0.77	0.53 (0.33 – 0.73)
HFD[2]	1.0059 (1.0052 – 1.0070)	1.0054 (1.0048 – 1.0066)	0.48	0.57 (0.38 – 0.77)
Skewness[2]	-0.02 (-0.05 – 0.04)	-0.03 (-0.05 – <-0.01)	0.25	0.62 (0.42 – 0.81)
Kurtosis[2]	0.20 (0.05 – 0.27)	0.17 (0.09 – 0.28)	0.86	0.52 (0.32 – 0.72)

EEG feature values are expressed as median (interquartile range); AUC = area under the receiver operating characteristic curve; HFD = Higuchi Fractal Dimension; LVO-a = anterior circulation large vessel occlusion; MSC = magnitude squared coherence; nDAR = normalized delta/alpha ratio; nDTABR = normalized (delta+theta)/(alpha+lower beta) ratio; nTAR = normalized theta/alpha ratio; pdBSI = pairwise derived Brain Symmetry Index; RAP = relative alpha power; RBP = relative lower beta power; RDP = relative delta power; RTP = relative theta power; SampEn = sample entropy; WPLI = weighted phase lag index.

[1] *p*-value for the difference between patients with and without an LVO-a stroke.

[2] calculated for the frequency band 1–18Hz.

corrected EEG signals and comparison of the EEG power spectra before and after correction. We furthermore evaluated the effect of artifact correction and detection on EEG feature values and their diagnostic accuracy for LVO-a stroke.

Results

The effect of the artifact correction and detection algorithm on multichannel data is shown in Figure 7. There are ocular artifacts visible in the raw data (Figure 7a) around $t = 0.8s$, $t = 3.9s$ and $t = 5.2s$. In Figure 7b it is seen that these artifacts are corrected, while the clean parts of the signals essentially remain unaffected. Besides the ocular artifacts a periodic artifact can be seen in the bipolar channel TPP9h–FFT9h. Even though the correction algorithm was only intended for ocular artifacts, the periodic artifact, most likely caused by the heart's electrical activity, is corrected as well.

In Figure 8 the effect of the correction algorithm is visualized in more detail for one bipolar EEG signal. In Figure 8a two large artifacts are present at $t = 0.9s$ and $t = 4.0s$. In Figure 8b the same EEG recording is shown but then with corrected artifacts. Additionally, around $t = 5.0s$ a small disturbance in the EEG signal has also been corrected. In Figure 8c and 8d the power of the raw and corrected EEG signals are visualized for different timestamps and frequencies. The difference between these plots is shown in Figure 8e. It can be seen that higher frequencies (>15Hz) in the signal are almost completely unaffected by the correction algorithm. Moreover, the power between the two large artifacts did not differ for the scenario in which artifacts were corrected and the scenario they were not.

The effect of artifact correction and detection on the calculated EEG features and the diagnostic accuracy is presented in Table 9. This table shows EEG feature values for patients with and without an LVO-a stroke, the corresponding p-values and the AUC for each feature. All these values are given for the following situations: no artifact correction or detection, only artifact detection and both artifact correction and detection. EEG features that were calculated in different frequency bands in the main body of this thesis are only listed for the frequency range 1–18 Hz.

The results for no artifact correction or detection and only artifact detection are similar; only small deviations in median feature values, interquartile range, p-values and AUC are seen. Only the pdBSI values of the non-LVO-a stroke patients changed considerably (0.34 [0.29–0.41) vs 0.24 [0.20–0.31]). For both the scenario with no artifact correction or detection and the scenario only artifact detection, several EEG features differ between patients with and without an LVO-a stroke: relative alpha and beta power, normalized DAR, TAR and DTABR, SampEn and HFD.

A great difference can be seen between the results obtained when only artifact detection is applied and the results when both artifact correction and detection are applied. Features which are higher for non-LVO-a stroke patients, are lower after artifact correction is applied, or vice versa. Several EEG features furthermore lose their significant difference due to artifact correction. After artifact correction and detection only the relative alpha power, DAR and pdBSI differ between patients with an LVO-a stroke and patients without (0.09 vs 0.12, p=0.01; 0.71 vs 0.61, p=0.01; 0.32 vs 0.26, p=0.01, respectively). Moreover, the diagnostic accuracy of all three features is improved after artifact correction is applied.

Discussion

In this appendix the effect of artifact correction and detection was determined. We showed that the artifact correction algorithm removes ocular artifacts from the EEG signals, while it leaves clean parts of the signals essentially unaffected. The algorithm is, however, not specific to ocular artifacts.

The values reported in Table 9 for the situation without artifact correction and detection and the situation with only artifact detection, are not always as we would expect. Reduced CBF results in a decrease in higher frequencies, followed by an increase in lower frequencies [4–7]. When no artifact correction is applied, the relative alpha and lower beta power are higher in LVO-a stroke patients than in non-LVO-a stroke patients (median = 0.23 vs 0.17 p=0.04 and median = 0.35 vs 0.28 p=0.05, respectively). The relative theta power is similar for both groups and the relative delta power is lower for LVO-a stroke patients, but this is not significant. Because the differences in relative delta, theta and lower beta power are in contradiction with our hypothesis, no logical results are seen for the DAR, TAR and DTABR either. When both artifact correction and detection are applied, the differences between LVO-a stroke and non-LVO-a stroke patients are more in line with our expectations and previous literature [8]. The relative theta power is, however, lower in LVO-a stroke patients and the relative lower beta power higher, although not statistically significant. A possible explanation of the strong influence of artifact correction on the EEG features of LVO-a stroke and non LVO-a stroke, would be the presence of more small (ocular) artifacts in the non-LVO-a stroke group. This has, nevertheless, not been evaluated quantitatively.

It is notable that complexity features, SampEn and HFD, both differ between LVO-a stroke and non-LVO-a stroke patients when no artifact correction is applied. The SampEn and HFD are both higher in LVO-a stroke patients (median = 0.35 vs 0.31 p=0.05 and median = 1.0077 vs 1.0072 p=0.05, respectively), which implies the signals of the LVO-a stroke patients are more complex. Previous literature suggests a decrease in CBF leads to reduced complexity of EEG signals [9–11]. However, no studies have been published on the SampEn and HFD in LVO-a stroke patients specifically. Once artifact correction is applied, the difference in complexity of the EEG signals between LVO-a stroke and non-LVO-a stroke patients is lost. This could be caused because there is a difference in the presence of small (ocular) artifacts between the groups, as was described in the previous paragraph. It could, nevertheless, also be the case that the EEG signals of LVO-a stroke patients are more complex and that the artifact correction algorithm diminishes the complexity of the signals. We suggest to evaluate the effect of the algorithm on the complexity of a clean EEG signal.

In conclusion, the artifact correction and detection algorithm removes (ocular) artifacts from the subhairline EEG signals. The algorithm moreover influences EEG feature values and thereby their diagnostic accuracy for LVO-a stroke. The diagnostic accuracy of several features is diminished, but the differences between the LVO-a stroke and non-LVO-a stroke patients are in better agreement with previous literature. The diagnostic accuracy of the relative alpha power, DAR and pdBSI is improved because of the artifact correction and detection algorithm.

References

[1] R. Ranjan, B. Chandra Sahana, and A. Kumar Bhandari, "Ocular artifact elimination from electroencephalography signals: A systematic review," *Biocybernetics and Biomedical Engineering*, vol. 41, no. 3, pp. 960–996, 2021.

[2] N. P. Castellanos and V. A. Makarov, "Recovering EEG brain signals: artifact suppression with wavelet enhanced independent component analysis," *Journal of Neuroscience Methods*, vol. 158, no. 2, pp. 300–312, 2006.

[3] M. F. Issa and Z. Juhasz, "Improved EOG artifact removal using wavelet enhanced independent component analysis," *Brain Sciences*, vol. 9, no. 12, p. 355, 2019.

[4] M. J. A. M. van Putten and J. Hofmeijer, "EEG monitoring in cerebral ischemia: Basic concepts and clinical applications," *Journal of Clinical Neurophysiology*, vol. 33, no. 3, pp. 203–210, 2016.

[5] B. Foreman and J. Claassen, "Quantitative EEG for the detection of brain ischemia," *Critical Care*, vol. 16, no. 2, p. 216, 2012.

[6] J. Wu, R. Srinivasan, E. Burke Quinlan, A. Solodkin, S. L. Small, and S. C. Cramer, "Utility of EEG measures of brain function in patients with acute stroke," *Journal of Neurophysiology*, vol. 115, no. 5, pp. 2399–2405, 2016.

[7] S. Finnigan, A. Wong, and S. Read, "Defining abnormal slow EEG activity in acute ischaemic stroke: Delta/alpha ratio as an optimal QEEG index," *Clinical Neurophysiology*, vol. 127, no. 2, pp. 1452–1459, 2016.

[8] L. C. C. van Meenen *et al.*, "Detection of large vessel occlusion stroke with electroencephalography in the emergency room: first results of the ELECTRA-STROKE study," *Journal of Neurology*, vol. 269, no. 4, pp. 2030–2038, 2021.

[9] S. Tong, B. Hong, L. Vigderman, and N. V. Thakor, "Subband EEG complexity after global hypoxic-ischemic brain injury," in *The 26th Annual International Conference of the IEEE Engineering in Medicine and Biology Society*, vol. 1, 2004, pp. 562–565.

[10] M. Rubega *et al.*, "EEG fractal analysis reflects brain impairment after stroke," *Entropy*, vol. 23, no. 5, 2021.

[11] F. Zappasodi, E. Olejarczyk, L. Marzetti, G. Assenza, V. Pizzella, and F. Tecchio, "Fractal dimension of EEG activity senses neuronal impairment in acute stroke," *PLOS ONE*, vol. 9, no. 6, e100199, 2014.

Appendix 3: Contralesional EEG features

Table 10: Contralesional EEG feature values of patients with and without an LVO-a stroke and the p-values of the Mann-Whitney U tests used to compare the EEG feature values. In case the patient did not have an ischemic stroke or TIA, the average feature value of both hemispheres was used.

	LVO-a stroke (n=13)	**Non-LVO-a stroke (n=21)**	**p-values**[1]
Frequency band power			
Relative delta power	0.51 (0.47 – 0.59)	0.53 (0.49 – 0.60)	0.65
Relative theta power	0.17 (0.16 – 0.18)	0.20 (0.16 – 0.24)	0.09
Relative alpha power	0.13 (0.11 – 0.15)	0.13 (0.10 – 0.15)	0.94
Relative lower beta power	**0.16 (0.14 – 0.20)**	**0.12 (0.08 – 0.14)**	**0.02**
Normalized DAR	0.56 (0.51 – 0.66)	0.61 (0.53 – 0.68)	0.72
Normalized TAR	0.19 (0.01 – 0.26)	0.23 (0.09 – 0.34)	0.39
Normalized DTABR	0.39 (0.28 – 0.51)	0.54 (0.38 – 0.59)	0.12
Functional connectivity			
MSC	0.18 (0.15 – 0.20)[2]	0.17 (0.16 – 0.19)[2]	0.90[2]
Delta	0.18 (0.16 – 0.19)	0.18 (0.17 – 0.20)	0.72
Theta	0.17 (0.15 – 0.18)	0.18 (0.16 – 0.20)	0.13
Alpha	0.16 (0.14 – 0.18)	0.18 (0.16 – 0.19)	0.34
Lower beta	0.16 (0.14 – 0.19)	0.16 (0.14 – 0.18)	0.75
WPLI	0.18 (-0.12 – 0.21)[2]	-0.06 (-0.22 – 0.02)[2]	0.43[2]
Delta	0.02 (-0.06 – 0.08)	-0.01 (-0.13 – 0.07)	0.27
Theta	0.01 (-0.10 – 0.18)	-0.09 (-0.19 – 0.08)	0.27
Alpha	0.04 (-0.10 – 0.21)	-0.06 (-0.14 – 0.13)	0.56
Lower beta	0.11 (-0.01 – 0.17)	<0.01 (-0.07 – 0.11)	0.13
Complexity			
Sample entropy	0.280 (0.257 – 0.293)[2]	0.245 (0.231 – 0.280)[2]	0.07[2]
Delta	0.060 (0.059 – 0.061)	0.061 (0.059 – 0.063)	0.21
Theta	0.211 (0.208 – 0.215)	0.217 (0.210 – 0.221)	0.17
Alpha	0.370 (0.365 – 0.377)	0.367 (0.363 – 0.373)	0.44
Lower beta	0.496 (0.491 – 0.500)	0.491 (0.489 – 0.499)	0.52
HFD	1.0065 (1.0060 – 1.0067)[2]	1.0054 (1.0044 – 1.0066)[2]	0.08[2]
Delta	**0.9933 (0.9928 – 0.9935)**	**0.9937 (0.9934 – 0.9940)**	**0.03**
Theta	0.9998 (0.9997 – 1.0000)	1.0000 (0.9996 – 1.0000)	0.58
Alpha	1.0037 (1.0035 – 1.0038)	1.0036 (1.0034 – 1.0037)	0.42
Lower beta	1.0103 (1.0101 – 1.0105)	1.0102 (1.0100 – 1.0104)	0.08
Probability distribution			
Skewness	-0.0163 (-0.0555 – 0.0064)[2]	-0.0116 (-0.0492 – 0.0020)[2]	0.84[2]
Delta	-0.0298 (-0.0500 – 0.0075)	-0.0049 (-0.0281 – 0.0070)	0.52
Theta	-0.0010 (-0.0046 – 0.0020)	-0.0012 (-0.0028 – 0.0006)	0.91
Alpha	<0.0001 (-0.0001 – 0.0001)	0.0001 (-0.0002 – 0.0002)	0.72
Lower beta	<-0.0001 (-0.0002 – 0.0001)	<-0.0001 (<-0.0002 – 0.0001)	0.56
Kurtosis	0.29 (0.12 – 0.40)[2]	0.19 (0.08 – 0.34)[2]	0.16[2]
Delta	0.27 (0.16 – 0.48)	0.20 (-0.02 – 0.32)	0.18
Theta	0.21 (0.11 – 0.50)	0.17 (0.04 – 0.31)	0.54
Alpha	0.19 (0.11 – 0.23)	0.12 (0.04 – 0.27)	0.40
Lower beta	0.08 (0.04 – 0.22)	0.16 (0.01 – 0.33)	0.69

EEG feature values are expressed as median (interquartile range); bold values denote statistical significance at a $p \leq 0.05$ level; DAR = delta/alpha ratio; DTABR = (delta+theta)/(alpha+lower beta) ratio; HFD = Higuchi fractal dimension; LVO-a = anterior circulation large vessel occlusion; MSC = magnitude squared coherence; pdBSI = pairwise derived Brain Symmetry Index; TAR = theta/alpha ratio; WPLI = weighted phase lag index.
[1] p-value for the difference between patients with and without an LVO-a stroke.
[2] Calculated for the frequency band 1–18Hz.

Table 11: The diagnostic accuracy for LVO-a stroke of the contralesional frequency band power and functional connectivity features. The diagnostic accuracy is expressed as the area under the ROC curve, sensitivity, specificity PPV and NPV.

	AUC (95% CI)	**Sensitivity (95% CI)**	**Specificity (95% CI)**	**PPV (95% CI)**	**NPV (95% CI)**
Frequency band power					
Relative delta power	0.55 (0.35–0.75)	15% (4%–42%)	83% (64%–93%)	33% (10%–70%)	65% (47%–79%)
Relative theta power	0.67 (0.48–0.86)	23% (8%–50%)	92% (74%–98%)	60% (23%–88%)	69% (51%–82%)
Relative alpha power	0.51 (0.31–0.71)	15% (4%–42%)	83% (64%–93%)	33% (10%–70%)	65% (47%–79%)
Relative lower beta power	0.74 (0.56–0.92)	54% (29%–77%)	83% (64%–93%)	64% (35%–84%)	77% (58%–89%)
Normalized DAR	0.53 (0.34–0.74)	23% (8%–50%)	88% (69%–96%)	50% (19%–81%)	68% (50%–81%)
Normalized TAR	0.59 (0.39–0.79)	38% (18%–64%)	83% (64%–93%)	56% (27%–81%)	71% (53%–85%)
Normalized DTABR	0.66 (0.47–0.85)	38% (18%–64%)	88% (69%–96%)	62% (31%–96%)	72% (54%–85%)
Functional connectivity					
MSC	0.52 (0.32–0.71)[1]	38% (18%–64%)[1]	87% (68%–95%)[1]	57% (25%–84%)[1]	69% (51%–83%)[1]
Delta	0.54 (0.34–0.73)	23% (8%–50%)	87% (68%–95%)	50% (18%–81%)	67% (49%–81%)
Theta	0.66 (0.46–0.85)	38% (18%–64%)	87% (68%–95%	62% (31%–86%)	71% (53%–85%)
Alpha	0.60 (0.40–0.80)	46% (23%–71%)	91% (73%–98%)	75% (41%–87%)	75% (57%–87%)
Lower beta	0.54 (0.34–0.74)	31% (13%–58%)	87% (68%–95%)	57% (25%–84%)	69% (51%–83%)
WPLI	0.58 (0.38–0.78)[1]	38% (18%–64%)[1]	96% (79%–99%)[1]	80% (38%–96%)[1]	71% (53%–85%)[1]
Delta	0.57 (0.37–0.77)	23% (8%–50%)	87% (68%–95%)	50% (19%–81%)	67% (49%–81%)
Theta	0.62 (0.42–0.81)	31% (13%–58%)	87% (68%–95%)	57% (25%–84%)	69% (51%–83%)
Alpha	0.56 (0.36–0.76)	31% (13%–58%)	87% (68%–95%)	57% (25%–84%)	69% (51%–83%)
Lower beta	0.66 (0.46–0.85)	31% (13%–58%)	96% (79%–99%)	80% (38%–96%)	71% (53%–84%)

AUC = area under the receiver operating characteristic curve; DAR = delta/alpha ratio; DTABR = (delta+theta)/(alpha+lower beta) ratio; CI = confidence interval; NPV = negative predictive value; pdBSI = pairwise derived Brain Symmetry Index; PPV = positive predictive value; TAR = theta/alpha ratio; WPLI = weighted phase lag index.
[1] Calculated for the frequency band 1–18Hz.

Table 12: The diagnostic accuracy for LVO-a stroke of the contralesional complexity and probability distribution features. The diagnostic accuracy is expressed as the area under the ROC curve, sensitivity, specificity PPV and NPV.

	AUC (95% CI)	**Sensitivity (95% CI)**	**Specificity (95% CI)**	**PPV (95% CI)**	**NPV (95% CI)**
Complexity					
SampEn	0.68 (049.–0.87)[1]	31% (13%–58%)[1]	83% (64%–93%)[1]	50% (22%–78%)[1]	69% (51%–83%)[1]
Delta	0.63 (0.43–0.82)	23% (8%–50%)	96% (78%–99%)	75% (30%–95%)	70% (53%–83%)
Theta	0.64 (0.45–0.83)	31% (13%–58%)	83% (64%–93%)	50% (22%–78%)	69% (51%–83%)
Alpha	0.58 (0.38–0.78)	38% (18%–64%)	92% (74%–98%)	71% (36%–92%)	73% (56%–86%)
Lower beta	0.57 (0.37–0.77)	15% (4%–42%)	83% (64%–93%)	33% (10%–70%)	65% (47%–79%)
HFD	0.68 (0.49–0.87)[1]	23% (8%–50%)[1]	88% (69%–96%)[1]	50% (19%–81%)[1]	68% (50%–81%)[1]
Delta	0.72 (0.54–0.90)	46% (23%–71%)	83% (64%–93%)	60% (31%–83%)	74% (55%–87%)
Theta	0.56 (0.36–0.76)	23% (8%–50%)	92% (74%–98%)	60% (23%–88%)	69% (51%–82%)
Alpha	0.58 (0.39–0.78)	23% (8%–50%)	83% (64%–93%)	43% (16%–75%)	67% (49%–81%)
Lower beta	0.60 (0.40–0.79)	38% (18%–64%)	88% (69%–96%)	62% (31%–86%)	72% (54%–85%)
Probability distribution					
Skewness	0.52 (0.41–0.80)[1]	31% (13%–58%)[1]	88% (69%–96%)[1]	57% (25%–84%)[1]	70% (52%–83%)[1]
Delta	0.57 (0.37–0.77)	15% (4%–42%)	88% (69%–96%)	40% (12%–77%)	66% (48%–80%)
Theta	0.51 (0.32–0.71)	38% (18%–64%)	88% (69%–96%)	62% (31%–86%)	72% (54%–85%)
Alpha	0.54 (0.34–0.74)	15% (4%–42%)	100% (86%–100%)	100% (34%–100%)	69% (52%–81%)
Lower beta	0.56 (0.36–0.76)	23% (8%–50%)	88% (69%–96%)	50% (19%–81%)	68% (50%–81%)
Kurtosis	0.64 (0.30–0.69)[1]	38% (18%–64%)[1]	92% (74%–98%)[1]	71% (36%–92%)[1]	73% (56%–86%)[1]
Delta	0.64 (0.44–0.83)	38% (18%–64%)	88% (69%–96%)	62% (31%–86%)	72% (54%–85%)
Theta	0.56 (0.37–0.76)	31% (13%–58%)	92% (74%–98%)	67% (30%–90%)	71% (53%–84%)
Alpha	0.59 (0.39–0.78)	15% (4%–42%)	96% (78%–99%)	67% (21%–94%)	68% (51%–81%)
Lower beta	0.54 (0.34–0.74)	15% (4%–42%)	83% (64%–93%)	33% (10%–70%)	65% (47%–79%)

AUC = area under the receiver operating characteristic curve; CI = confidence interval; HFD = Higuchi fractal dimension; NPV = negative predictive value; PPV = positive predictive value; SampEn = sample entropy.
[1] Calculated for the frequency band 1–18Hz.

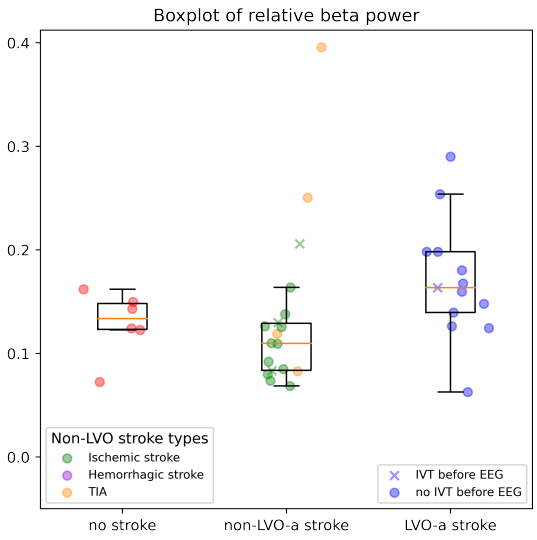

(a)

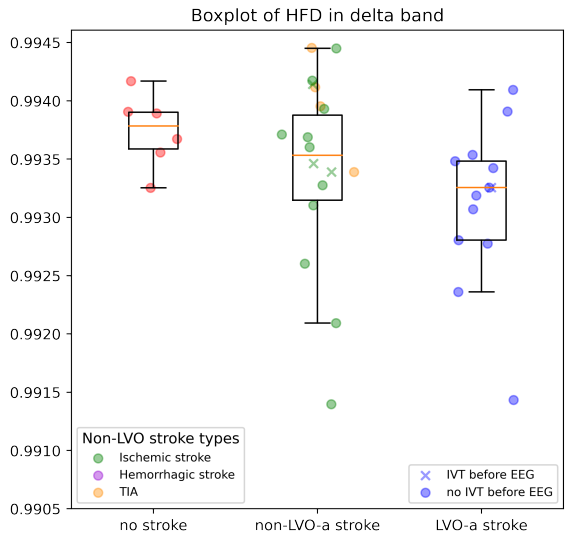

(b)

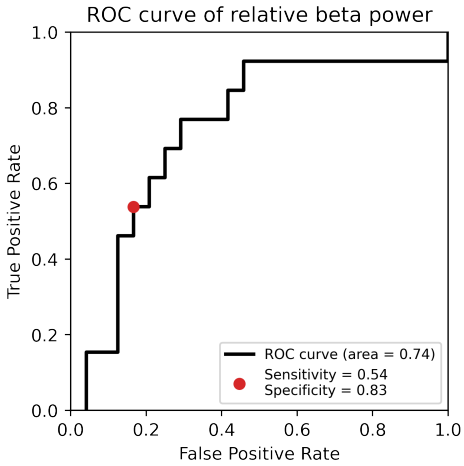

(c)

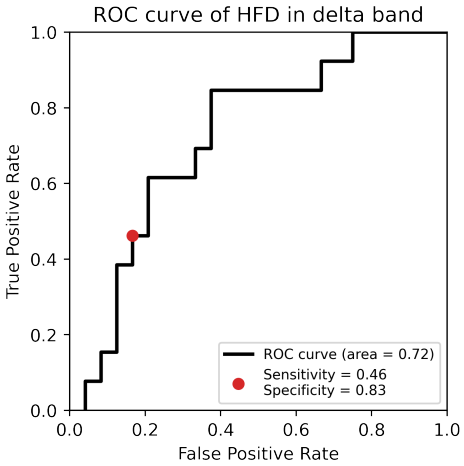

(d)

Figure 9: Boxplots and ROC curves of the contralesional relative beta power and HFD in the delta frequency band; (a and b) the average feature values are shown for patients without a stroke, with a non-LVO-a stroke and with a LVO-a stroke; (c and d) optimal cut-off point (red dot) was determined as the maximum sensitivity at a specificity of 80% for LVO-a stroke.

Appendix 4: Diagnostic accuracy of all ipsilesional EEG features

Table 13: The diagnostic accuracy for LVO-a stroke of the ipsilesional frequency band power, frequency asymmetry and functional connectivity features. The diagnostic accuracy is expressed as the area under the ROC curve, sensitivity, specificity PPV and NPV.

	AUC (95% CI)	**Sensitivity (95% CI)**	**Specificity (95% CI)**	**PPV (95% CI)**	**NPV (95% CI)**
Frequency band power					
Relative delta power	0.65 (0.46–0.84)	38% (18%–64%)	92% (74%–98%)	71% (36%–92%)	73% (56%–86%)
Relative theta power	0.65 (0.46–0.84)	23% (8%–50%)	92% (74%–98%)	60% (23%–88%)	69% (51%–82%)
Relative alpha power	0.76 (0.58–0.93)	69% (42%–87%)	88% (69%–96%)	75% (47%–91%)	84% (65%–94%)
Relative lower beta power	0.53 (0.33–0.73)	38% (18%–64%)	83% (64%–93%)	56% (27%–81%)	71% (53%–85%)
Normalized DAR	0.75 (0.58–0.82)	62% (36%–82%)	88% (69%–96%)	73% (43%–90%)	81% (62%–91%)
Normalized TAR	0.59 (0.39–0.78)	31% (13%–58%)	88% (69%–97%)	73% (43%–90%)	81% (62%–91%)
Normalized DTABR	0.57 (0.37–0.77)	31% (13%–58%)	96 (78%–99%)	80% (38%–96%)	72% (55%–84%)
Frequency asymmetry					
pdBSI	0.75 (0.57–0.92)[1]	46% (23%–71%)[1]	88% (69%–96%)[1]	67% (35%–88%)[1]	75% (57%–87%)[1]
Delta	0.73 (0.55–0.91)	46% (23%–71%)	92% (74%–98%)	75% (41%–93%)	76% (58%–88%)
Theta	0.88 (0.76–1.00)	85% (58%–96%)	83% (64%–93%)	73% (48%–89%)	91% (72%–97%)
Alpha	0.74 (0.56–0.92)	62% (36%–82%)	88% (69%–96%)	73% (43%–90%)	81% (62%–91%)
Lower beta	0.58 (0.38–0.78)	38% (18%–64%)	83% (64%–93%)	56% (27%–81%)	71% (53%–85%)
Functional connectivity					
MSC	0.58 (0.37–0.78)[1]	33% (14%–61%)[1]	83% (64%–93%)[1]	50% (22%–78%)[1]	71% (53%–78%)[1]
Delta	0.68 (0.48–0.87)	50% (25%–75%)	83% (64%–93%)	60% (31%–83%)	77% (58%–89%)
Theta	0.61 (0.41–0.81)	42% (19%–68%)	88% (69%–96%)	62% (31%–86%)	75% (57%–87%)
Alpha	0.58 (0.38–0.86)	33% (14%–61%)	92% (74%–98%)	67% (30%–90%)	73% (56%–86%)
Lower beta	0.58 (0.37–0.78)	42% (19%–68%)	83% (64%–93%)	56% (27%–81%)	74% (55%–97%)
WPLI	0.64 (0.44–0.84)[1]	42% (19%–68%)[1]	88% (69%–96%)[1]	62% (31%–86%)[1]	75% (57%–87%)[1]
Delta	0.65 (0.45–0.85)	25% (9%–53%)	88% (69%–96%)	50% (19%–81%)	70% (52%–83%)
Theta	0.61 (0.41–0.81)	50% (25%–75%)	83% (64%–93%)	60% (31%–83%)	77% (58%–89%)
Alpha	0.53 (0.33–0.74)	17% (5%–45%)	83% (64%–93%)	33% (10%–70%)	67% (49%–81%)
Lower beta	0.60 (0.40–0.80)	17% (5%–45%)	92% (74%–98%)	50% (15%–85%)	69% (51%–82%)

AUC = area under the receiver operating characteristic curve; DAR = delta/alpha ratio; DTABR = (delta+theta)/(alpha+lower beta) ratio; CI = confidence interval; NPV = negative predictive value; pdBSI = pairwise derived Brain Symmetry Index; PPV = positive predictive value; TAR = theta/alpha ratio; WPLI = weighted phase lag index.
[1] calculated for the frequency band 1–18Hz.

Table 14: The diagnostic accuracy for LVO-a stroke of the ipsilesional complexity and probability distribution features. The diagnostic accuracy is expressed as the area under the ROC curve, sensitivity, specificity PPV and NPV.

	AUC (95% CI)	**Sensitivity (95% CI)**	**Specificity (95% CI)**	**PPV (95% CI)**	**NPV (95% CI)**
Complexity					
SampEn	0.53 (0.33–0.73)[1]	31% (13%–58%)[1]	83% (64%–93%)[1]	50% (22%–78%)[1]	69% (51%–83%)[1]
Delta	0.60 (0.40–0.79)	38% (18%–64%)	88% (69%–96%)	62% (31%–86%)	72% (54%–85%)
Theta	0.68 (0.49–0.87)	46% (23%–71%)	92% (74%–98%)	75% (41%–93%)	76% (58%–88%)
Alpha	0.67 (0.48–0.86)	46% (23%–71%)	88% (69%–96%)	67% (35%–88%)	75% (57%–87%)
Lower beta	0.64 (0.45–0.84)	46% (23%–71%)	83% (64%–93%)	60% (31%–83%)	74% (55%–87%)
HFD	0.57 (0.38–0.77)[1]	31% (13%–58%)[1]	83% (64%–93%)[1]	50% (22%–78%)[1]	69% (51%–83%)[1]
Delta	0.64 (0.26–0.83)	62% (36%–82%)	83% (64%–93%)	67% (39%–86%)	80% (61%–91%)
Theta	0.55 (0.35–0.75)	23% (8%–50%)	96% (80%–99%)	75% (30%–95%)	70% (53%–83%)
Alpha	0.58 (0.39–0.78)	31% (13%–58%)	88% (69%–96%)	57% (25%–84%)	70% (52%–83%)
Lower beta	0.64 (0.45–0.83)	38% (18%–64%)	83% (64%–93%)	56% (27%–81%)	71% (53%–85%)
Probability distribution					
Skewness	0.62 (0.42–0.81)[1]	46% (23%–71%)[1]	88% (69%–96%)[1]	67% (35%–88%)[1]	75% (57%–87%)[1]
Delta	0.51 (0.31–0.70)	23% (8%–50%)	92% (74%–98%)	60% (23%-88%)	69% (51%–82%)
Theta	0.53 (0.33–0.73)	23% (8%–50%)	83% (64%–93%)	43% (16%–75%)	67% (49%–81%)
Alpha	0.54 (0.34–0.74)	38% (18%–64%)	83% (64%–93%)	56% (27%–81%)	71% (53%–85%)
Lower beta	0.70 (0.51–0.88)	46% (23%–71%)	83% (64%–93%)	60% (31%–83%)	74% (55%–87%)
Kurtosis	0.52 (0.32–0.72)[1]	31% (13%–58%)[1]	83% (64%–93%)[1]	50% (22%–78%)[1]	69% (51%–83%)[1]
Delta	0.58 (0.38–0.77)	23% (8%–50%)	96% (80%–99%)	75% (30%–95%)	70% (53%–83%)
Theta	0.54 (0.34–0.74)	23% (8%–50%)	88% (69%–96%)	50% (19%–81%)	68% (50%–81%)
Alpha	0.50 (0.31–0.70)	23% (8%–50%)	83% (64%–93%)	43% (16%–75%)	67% (49%–81%)
Lower beta	0.58 (0.39–0.78)	15% (4%–42%)	83% (64%–93%)	33% (10%–70%)	65% (47%–79%)

AUC = area under the receiver operating characteristic curve; CI = confidence interval; HFD = Higuchi fractal dimension; NPV = negative predictive value; PPV = positive predictive value; SampEn = sample entropy.
[1] calculated for the frequency band 1–18Hz.

Appendix 5: Performance logistic regression model using individual EEG features

Table 15: The diagnostic accuracy for LVO-a stroke of the ipsilesional frequency band power, frequency asymmetry and functional connectivity features, as determined by a LR model. The diagnostic accuracy is expressed as the area under the ROC curve, sensitivity, specificity PPV and NPV.

	Accuracy (95% CI)	Sensitivity (95% CI)	Specificity (95% CI)	PPV (95% CI)	NPV (95% CI)
Frequency band power					
Relative delta power	56% (42%–69%)	54% (35%–72%)	58% (39%–76%)	57% (37%–74%)	56% (37%–73%)
Relative theta power	56% (42%–69%)	67% (47%–82%)	46% (28%–65%)	55% (38%–72%)	58% (36%–77%)
Relative alpha power	71% (57%–82%)	83% (64%–93%)	58% (39%–76%)	67% (49%–81%)	78% (55%–91%)
Relative lower beta power	0% (0%–8%)	0% (0%–14%)	0% (0%–14%)	0% (0%–14%)	0% (0%–14%)
Normalized DAR	71% (57%–82%)	83% (64%–93%)	58% (39%–76%)	67% (49%–81%)	78% (55%–91%)
Normalized TAR	60% (46%–73%)	71% (51%–85%)	50% (31%–69%)	59% (41%–74%)	63% (41%–81%)
Normalized DTABR	52% (38%–66%)	58% (39%–76%)	46 (28%–65%)	52% (34%–69%)	52% (32%–72%)
Frequency asymmetry					
pdBSI	65% (50%–77%)[1]	63% (43%–79%)[1]	67% (47%–82%)[1]	65% (45%–81%)[1]	64% (45%–80%)[1]
Delta	67% (53%–78%)	54% (35%–72%)	79% (60%–91%)	72% (49%–88%)	63% (46%–78%)
Theta	73% (59%–83%)	67% (47%–82%)	79% (60%–91%)	76% (55%–89%)	70% (52%–84%)
Alpha	60% (46%–73%)	58% (39%–76%)	63% (43%–79%)	61% (41%–78%)	60% (41%–77%)
Lower beta	0% (0%–7%)	0% (0%–14%)	0% (0%–14%)	0% (0%–14%)	0% (0%–14%)
Functional connectivity					
MSC	52% (38%–66%)[1]	46% (28%–65%)[1]	58% (39%–76%)[1]	52% (33%–71%)[1]	52% (33%–70%)[1]
Delta	65% (50%–77%)	54% (35%–72%)	75% (55%–88%)	68% (46%–85%)	62% (44%–77%)
Theta	56% (42%–69%)	50% (31%–69%)	63% (43%–79%	57% (37%–76%)	56% (37%–72%)
Alpha	33% (22%–47%)	29% (15%–49%)	38% (21%–57%)	32% (16%–53%)	56% (37%–72%)
Lower beta	52% (38%–66%)	50% (31%–69%)	54% (35%–72%)	52% (33%–71%)	52% (33%–70%)
WPLI	46% (33%–60%)[1]	33% (18%–53%)[1]	58% (39%–76%)[1]	44% (25%–66%)[1]	47% (30%–64%)[1]
Delta	48% (34%–62%)	50% (31%–69%)	46% (28%–65%)	48% (30%–67%)	48% (29%–67%)
Theta	52% (38%–66%)	50% (31%–69%)	54% (35%–72%)	52% (33%–71%)	52% (33%–70%)
Alpha	40% (27%–54%)	46% (28%–65%)	33% (18%–53%)	41% (25%–59%)	38% (21%–59%)
Lower beta	44% (31%–58%)	42% (24%–61%)	46% (28%–65%)	43% (26%–63%)	44% (27%–63%)

AUC = area under the receiver operating characteristic curve; DAR = delta/alpha ratio; DTABR = (delta+theta)/(alpha+lower beta) ratio; CI = confidence interval; NPV = negative predictive value; pdBSI = pairwise derived Brain Symmetry Index; PPV = positive predictive value; TAR = theta/alpha ratio; WPLI = weighted phase lag index.

[1] calculated for the frequency band 1–18Hz.

Table 16: The diagnostic accuracy for LVO-a stroke of the ipsilesional complexity and probability distribution features, as determined by a LR model. The diagnostic accuracy is expressed as the area under the ROC curve, sensitivity, specificity PPV and NPV.

	Accuracy (95% CI)	**Sensitivity (95% CI)**	**Specificity (95% CI)**	**PPV (95% CI)**	**NPV (95% CI)**
Complexity					
SampEn	48% (34%–62%)[1]	46% (28%–65%)[1]	50% (31%–69%)[1]	48% (29%–67%)[1]	48% (30%–67%)[1]
Delta	46% (33%–60%)	54% (35%–72%)	38% (21%–57%)	46% (30%–64%)	45% (26%–66%)
Theta	63% (48%–75%)	67% (47%–82%)	58% (39%–76%)	62% (43%–78%)	64% (43%–80%)
Alpha	54% (40%–67%)	46% (28%–65%)	63% (43%–79%)	55% (34%–74%)	54% (36%–70%)
Lower beta	66% (53%–78%)	75% (55%–88%)	58% (39%–76%)	64% (46%–79%)	70% (48%–85%)
HFD	52% (38%–66%)[1]	50% (31%–69%)[1]	54% (35%–72%)[1]	52% (33%–71%)[1]	52% (33%–70%)[1]
Delta	44% (31%–58%)	50% (31%–69%)	38% (21%–57%)	44% (28%–63%)	43% (24%–63%)
Theta	38% (25%–52%)	29% (15%–49%)	46% (28%–65%)	35% (18%–57%)	39% (24%–58%)
Alpha	33% (22%–47%)	42% (25%–61%)	25% (12%–45%)	30% (15%–52%)	30% (15%–52%)
Lower beta	56% (42%–69%)	63% (43%–79%)	50% (31%–69%)	56% (37%–72%)	57% (37%–76%)
Probability distribution					
Skewness	48% (34%–62%)[1]	46% (28%–65%)[1]	50% (31%–69%)[1]	48% (29%–67%)[1]	48% (30%–67%)[1]
Delta	44% (31%–58%)	54% (35%–72%)	33% (18%–53%)	45% (28%–62%)	42% (23%–64%)
Theta	2% (0%–10%)	0% (0%–14%)	4% (0%–20%)	0% (0%–14%)	4% (0%–20%)
Alpha	42% (29%–56%)	29% (15%–49%)	54 (35%–72%)	39% (20%–61%)	43% (27%–61%)
Lower beta	63% (48%–75%)	54% (35%–72%)	71% (51%–85%)	65% (43%–82%)	61% (42%–76%)
Kurtosis	38% (25%–52%)[1]	38% (21%–57%)[1]	38% (21%–57%)[1]	38% (21%–57%)[1]	38% (21%–57%)[1]
Delta	48% (34%–62%)	42% (24%–61%)	54% (35%–72%)	48% (28%–68%)	48% (31%–66%)
Theta	0% (0%–7%)	0% (0%–14%)	0% (0%–14%)	0% (0%–14%)	0% (0%–14%)
Alpha	35% (23%–50%)	17% (7%–36%)	54% (35%–72%)	27% (11%–52%)	39% (25%–56%)
Lower beta	58% (44%–71%)	67% (47%–82%)	50% (31%–69%)	57% (39%–73%)	60% (39%–78%)

AUC = area under the receiver operating characteristic curve; CI = confidence interval; HFD = Higuchi fractal dimension; NPV = negative predictive value; PPV = positive predictive value; SampEn = sample entropy.
[1] calculated for the frequency band 1–18Hz.